A *MEF2C* transcripton factor network regulates proliferation of glomerular endothelial cells in diabetic kidney disease

Ricardo Melo Ferreira[1], Debora L. Gisch[1], Carrie L. Phillips[1], Ying-Hua Cheng[1], Maansi Asthana[1], Blue B. Lake[2], William S. Bowen[1], Fang Fang[1], Mahla Ashgari[1], Angela Sabo[1], Daria Barwinska[1], Michael J. Ferkowicz[1], Robert D. Toto[3], John R. Sedor[4], Sylvia E. Rosas[5], Petter Bjornstad[6], Jeffrey B Hodgin[10], Charles E. Alpers[7], Pinaki Sarder[8], Jonathan Himmelfarb[9], Jennifer A. Schaub[10], Viji Nair[10], Seth Winfree[11], Timothy A. Sutton[1], Katherine J. Kelly[1], The Kidney Precision Medicine Project, Matthias Kretzler[10], Sanjay Jain[12], Tarek M. El-Achkar[1], Pierre C. Dagher[1], Michael T. Eadon[1]

1 Department of Medicine, Indiana University School of Medicine, Indianapolis, IN, 46202, USA

2 Department of Bioengineering, University of California, La Jolla, CA, 92093, USA

Present address: San Diego Institute of Science, Altos Labs, San Diego, CA, USA

3 Department of Medicine, University of Texas Southwestern, Dallas, TX, 75390, USA

4 Department of Medicine, Cleveland Clinic, Cleveland, OH, 44195, USA

5 Joslin Diabetes Center, Harvard Medical School, Boston, MA 02215, USA

6 University of Washington Medicine Diabetes Institute, University of Washington, Seattle, WA 98109, USA

7 Department of Pathology, University of Washington, Seattle, WA 98195, USA

8 Department of Biomedical Engineering, University of Florida, Gainesville, FL , 32603, USA

9 Department of Medicine, Mount Sinai School of Medicine, New York, NY, 10029, USA

10 Department of Medicine, University of Michigan, Ann Arbor, MI 48109, USA

11 National Institute of Health, Bethesda, MD, 20892, USA

12 Department of Medicine, Washington University in Saint Louis, St. Louis, MO 63103, USA

Running title: Endothelial and mesangial cell regulation in diabetes

Key Words: semaphorin 6A, plexin A2, niche, nodular mesangial glomerulosclerosis, spatial transcriptomics, open chromatin, epigenetics

Corresponding information:

Michael T Eadon, MD
Indiana University School of Medicine, Department of Medicine
Tel: 317-274-2821
E-mail: meadon@iu.edu

Abstract

Background:

The maintenance of a healthy epithelial-endothelial juxtaposition requires cross-talk within glomerular cellular niches. Neovascularization and nodular mesangial sclerosis are manifestations of dysregulated communication in diabetic kidney disease (DKD). We sought to understand the spatially-anchored regulation and transition of endothelial and mesangial cells from health to injury in DKD.

Methods:

From 77 human kidney biopsy samples, an integrated multi-omics approach was leveraged to identify cellular niches, cell-cell communication, cell injury trajectories, and regulatory transcription factor (TF) networks in glomerular endothelial and mesangial cells. Data were culled from single nucleus RNA sequencing, single nucleus ATAC sequencing, and three orthogonal spatial transcriptomic technologies and correlated with histopathological and clinical trial data.

Results:

We identified a cellular niche of the diabetic glomerulus enriched in a proliferative endothelial cell sub type (prEC) and altered vascular smooth muscle cells (VSMCs). Cellular communication within this niche maintained pro-angiogenic signaling with loss of anti-angiogenic factors. We identified a TF network of *MEF2C*, *MEF2A*, and *TRPS1* which regulated *SEMA6A* and *PLXNA2*, a receptor-ligand pair opposing angiogenesis. *In silico* knockout of the TF network disrupted the transition from a healthy glomerular capillary endothelial cell (EC-GC) to a prEC, with concomitant acceleration toward a degenerative (injury) endothelial phenotype. Glomeruli enriched in the prEC niche had histologic evidence of neovascularization. A pro-fibrotic niche mapped in segmentally sclerotic DKD glomeruli. *MEF2C* activity was increased in diabetic glomeruli and more so in glomeruli with nodular mesangial sclerosis. The gene regulatory network (GRN) of *MEF2C* was dysregulated in EC-GCs of patients with DKD, but sodium glucose trasporter-2 inhibitor (SGLT2i) treatment reversed the *MEF2C* GRN effects of DKD.

Conclusions:

The *MEF2C*, *MEF2A*, and *TRPS1* TF network carefully balances the fate of the EC-GC in DKD. When the TF network is “on” or over-expressed in DKD, EC-GCs may progress to a prEC state, while TF suppression leads to cell death. prEC abundance and signaling underlie neovascularization in DKD. SGLT2i therapy shows promise in restoring he balance of *MEF2C* activity in DKD.

Introduction

Diabetic Kidney Disease (DKD) is the leading cause of Chronic Kidney Disease (CKD), affecting over 12 million individuals in the United States[1]. Early manifestations of DKD include thickening of the glomerular basement membrane and mesangial matrix expansion. As Heptinstall and others have noted, podocyte effacement and neovascularization with increased endothelial density materialize as DKD advances[2]. Late stage DKD is characterized by Kimmelstiel-Wilson (KW) nodule formation, podocyte loss, and glomerulosclerosis[3]. While podocyte injury in DKD is well described [4], a knowledge gap persists regarding the relationship between nodular mesangial sclerosis and neovascularization. Manifestations of DKD such as glomerular hypertension, hypoxia, and hyperglycemia all contribute to a complex milieu wherein the glomerular cell composition and communication change in response to stress[5]. Recently, a single-cell RNA sequencing (scRNAseq) study yielded an atlas of renal endothelial cells with key insights into blood pressure regulation[6]. However, glomerular response to stress is heterogeneous[7], with localized histologic changes. Therefore, the spatial context will augment our understanding of DKD pathophysiology[8].

Glomerular hypertension is a hallmark of DKD and may result in localized hypoxia[9]. Glomerular pressure is regulated distinctly from systemic blood pressure. Both hemodynamic changes and hormonal signaling drive glomerular hypertrophy and angiogenesis to compensate for hypoxia[9]. Vascular Endothelial Growth Factor A (VEGFA) expression within the glomerulus is necessary to maintain a healthy microvasculature[10]. VEGFA and B are upregulated in early DKD and their loss contributes to endothelial and mesangial cell defects[11], ultimately exacerbating proteinuria and glomerulosclerosis in murine models[10]; however, inhibition of VEGFB failed to reduce proteinuria in a Phase II trial[12]. A diversity of receptor-ligand pairs has been invoked to regulate cross-talk between the podocyte, endothelial cell, and mesangial cell. These signaling pathways include those initiated by angiopoietin, platelet-derived growth factor-β (*PDGFB*), and transforming growth factor-β[5].

Recently, we described a case of neovascularization in a patient with DKD[13]. In this case, three-dimensional CD31 protein staining confirmed the multiple afferent arterioles and pericapsular neovessels observed histologically. The increase in endothelial cell density was accompanied by upregulation of angiogenic gene expression assessed by spatial transcriptomics (ST). We expand upon this study by now interrogating all reference and DKD samples within the Kidney Precision Medicine Project (KPMP) and Human Biomolecular Atlas Program (HuBMAP) sc/snRNA-seq and Visium ST atlas of the kidney[14]. Using deconvolution tactics, we have previously defined colocalizing cell types with their attendant injury signatures and cellular cross-talk[15,16]. While progress has been made in cataloging proximal tubule cell transitions[17], including transcription factor (TF) networks that regulate phenotypic alterations in cellular response to injury[17], these approaches may also yield insights into the glomerular cell changes of DKD to define patient subgroups for targeted therapy. In this study, we hypothesized that spatial localization and cell communication would underlie the endothelial and vascular smooth muscle cell signature alterations associated with neovascularization and nodular mesangial sclerosis. To this end, we utilized orthogonal snRNA-seq and multiome atlases with three spatial transcriptomic datasets to better define the changes in the glomerular cell composition, expression, localization, communication, and regulation in the histologic context of DKD.

Methods

Sample acquisition: For Visium fresh frozen spatial transcriptomics, kidney biopsy samples were obtained with informed consent through the KPMP consortium (https://KPMP.org) and approved under a single Institutional Review Board (IRB #20190213) protocol at the University of Washington. Formalin-fixed paraffin-embedded (FFPE) samples were obtained under waiver of informed consent from the Biopsy Biobank Cohort of Indiana (BBCI)[18], approved by the Indiana University IRB (#1906572234), and by the Kidney Translational Research Center (KTRC) as part of the HuBMAP consortium under IRB #201102312 at Washington University in St. Louis. Samples were classified as DKD according to the clinical diagnosis at the time of biopsy (Supplemental Table S1).

Visium fresh frozen spatial transcriptomics: Kidney tissue preserved in Optimal Cutting Temperature compound (OCT) was obtained through the KPMP and processed following a standardized KPMP protocol[19]. Sections of 10 µm thickness were placed on a Visium barcoded slide and stained with hematoxylin (Sigma Aldrich Cat# HHS16) and eosin (Sigma Aldrich Cat# HT110380, H&E). Brightfield images were captured on a Keyence BZ-X810 microscope with a Nikon ×10 CFI Plan Fluor objective. Tissue was permeabilized for 12 minutes and mRNA was captured in the slide's barcoded spots. The library was prepared following the vendor's protocol (Visium CG000239 protocol) and sequenced on an Illumina NovaSeq 6000. Reads were aligned to reference genome GRCh38 2020-A and counts matrices were generated with Spaceranger 2.0.0.

Visium FFPE spatial transcriptomics: FFPE tissue was obtained from the BBCI[18]. A 7 µm section underwent the Visium FFPE pipeline, while a sequential 3 µm section underwent periodic acid-Schiff (PAS) staining. The 7 µm section was stained with H&E and aligned with a Visium slide using CytAssyst. The tissue was permeabilized and library prepared following the 10x Genomics protocol. The library underwent Illumina sequencing and the resulting reads were mapped to reference genome GRCh38 2020-A with the probeset 2.0 using Spaceranger 2.0.1.

Single Nucleus RNA sequencing analysis: The single nucleus RNA sequencing (snRNAseq) dataset was obtained from the published KPMP-HuBMAP atlas[14]. Samples annotated as papilla or medulla were excluded from the analysis. To reflect an inclusive set of cell types potentially localizing to glomeruli, all podocyte (POD), endothelial cell (EC), mesangial (MC) and Vascular Smooth Muscle cell (VSMC) nuclei (N=16,488) were co-clustered and re-annotated from this atlas[14]. Endothelial cells of the glomerular capillary remained annotated as EC-GC. Degenerative endothelial and degenerative peritubular capillary endothelial cells were annotated as dEC, while other endothelial cells (Afferent / Efferent Arteriole, Ascending Vasa Recta, Descending Vasa Recta, Peritubular Capillary, Cycling Endothelial, and Lymphatic) were annotated as Endothelial Cell – Not Specified (EC-NS). Degenerative vascular smooth muscle cells were annotated as dVSMC, while, the remaining vascular smooth muscle cells or pericytes (Renin-positive juxtaglomerular granular cells, vascular smooth muscle cell, vascular smooth muscle cell / pericyte) were annotated as Vascular Smooth Muscle Cells – Not Specified (VSMC-NS). After downstream analyses, a portion of EC-NS was classified as proliferative Endothelial Cells (prEC). A glomerular dataset was generated by subsetting the snRNAseq atlas to include these cell types. Nuclei were clustered correcting for batch effect with Harmony 1.2.0[20]. Cell-cell communications were predicted in the snRNAseq glomerular dataset using the package CellChat 2.1.2[21]

Visium data analysis: Within each Visium technology, OCT or FFPE, all samples were merged into a single object. Raw reads were normalized with SCTransform to correct for batch effects[16]. To define glomerular spots, glomeruli were manually annotated using the accompanying histological image and expression of *NPHS2*. Visium spots were assigned to a glomerulus if its center was located inside the annotated glomerulus. Due to the 55 µm diameter of each spot, periglomerular cells were still captured. To remove edge artifacts, the outermost layer of spots on the edge of the samples was excluded. Downstream analyses were conducted on the remaining spots. To estimate cell type composition in Visium Spatial Transcriptomics (ST), the expression of each spot is deconvolved using transfer scores from atlas annotations, calculated using the anchors' integration method from Seurat 4.3.3[22].

Xenium In Situ Sequencing (ISS): ISS captures RNA transcripts at subcellular resolution, allowing classification of single cells by cell specific markers. FFPE preserved tissue obtained from BBCI or HuBMAP was sectioned and placed on a Xenium slide and processed according to the manufacturer protocol (CG000582 Rev D and CG000584 Rev B). A custom probe set (BMU84Y, Supplemental Table S2) was designed to localize kidney cell types and injury patterns. To obtain histological images, standard staining procedures were followed with H&E staining and destaining, before dehydration and mounting with Eukitt mounting media (Electron Microscopy Sciences Cat #15320). Images were obtained on a Keyence microscope as described above. Histological images were registered to DAPI-stained nuclei images with Xenium Explorer 2.0.0. To identify cells in ISS, a subset of the snRNAseq dataset was mapped with the anchors' method of Seurat 5.0.3. Epithelial and stromal degenerative cell states were overrepresented due to the limited probe panel and excluded from mapping. All glomerular cell types described in the manuscript were maintained.

Differential Expression and Pathway Enrichment: Differential gene expression between sets of nuclei or spots was calculated using a Wilcox rank sum test. The significance threshold was set at 0.05 for p values after adjustment with a Bonferroni correction. Pathway enrichment for snRNAseq and ST clusters was performed with SCPA 1.6.1[23]. Single cell groups were defined *a priori* In this pathway analysis method. Then, for each pathway, the cells are clustered according only to the expression of the pathway's genes, and a q-value is attributed according to the similarity of the clustering to the predetermined groups.

Cellular niches: Cellular niches were defined by clustering ST spots according to their cell type composition using traditional Louvain clustering and UMAP projection methods from Seurat. A Fisher's exact test was utilized to evaluate the likelihood of each cellular niche being overrepresented in DKD samples.

Annotation of proliferative Endothelial Cells (prEC): Differential expression between endothelial niches in reference and DKD ST samples identified genes potentially representative of prECs. Reversing the Seurat anchors method which transferred snRNAseq labels to the ST, we next back-mapped the ST niche annotations to the glomerular cells of the multiome dataset to identify an endothelial subgroup preferentially mapping to the DKD endothelial ST niche. This cluster was validated by the expression of differentially expressed genes between the niches. The prEC annotation was then mapped onto the snRNAseq atlas for receptor-ligand modeling.

Multiome analysis: The multiome data were obtained from the KPMP-HuBMAP epigenetic atlas[17]. The Seurat object was subsetted to the same cell types as the snRNA-seq dataset with 4410 cells and 983,017 peaks annotated by MACs2. After processing, data were normalized, highly variable features identified, and dimensionality reduction performed through techniques like PCA. The batch effect was removed by harmony (v.1.2.0). The metadata motif database used was JASPAR2022 (v.0.99.7). scMEGA (v.1.0.2) was employed to correlate gene expression with chromatin accessibility at regulatory elements, enabling the modeling of cell trajectories and the identification of regulatory interactions[24]. The *in silico* knockout was modeled with CellOracle (v.0.12.0) using the GRN generated by scMEGA. CellOracle's simulation tools predicted the downstream effects on target genes and cell states, allowing us to infer the regulatory impact of TF loss[25].

Histopathological scoring of Visium FFPE samples: Each glomerulus in the Visium FFPE dataset was annotated in the sequential H&E (7 µm) and PAS (3 µm) images. Individual glomeruli were scored according to the categorial presence of the following histopathological features: hilar neovascularization; non-nodular mesangial sclerosis (mesangial expansion); nodular mesangial sclerosis (Kimmelstiel-Wilson nodule); and segmental glomerular sclerosis (SGS). To evaluate the association with histopathologic category, a Fisher's exact test assessed niche mapping proportion and a student's t-test was used for *MEF2C* activity.

SGLT2 inhibitor analysis: The differential expression of genes regulated by *MEF2C* was assessed in the endothelial cluster of a human kidney scRNAseq dataset[26] for three conditions 1) healthy reference tissue, 2) youth with type 2 diabetes without sodium glucose transporter 2 inhibitor (SGLT2i), or 3) youth with type 2 diabetes with SGLT2i. Fold changes of differentially expressed genes (after multiple-testing adjustment) were depicted in a heatmap.

Results

Subjects

Nodular mesangial sclerosis and neovascularization are common manifestations of DKD. To elucidate the cellular cross-talk underlying the spectrum of DKD within the glomerulus, we interrogated orthogonal data derived from a partially overlapping set of kidney samples (Supplemental Table S1). The total number of human kidney specimens interrogated was 77 including snRNAseq (N= 29), the multiome combined snRNA-seq and scATAC-seq (N= 12), 10x Visium fresh frozen spatial transcriptomics (N= 36 samples [14 reference, 22 DKD], 31545 spots), FFPE ST (N= 12 samples [8 reference, 4 DKD], 22052 spots), and Xenium *in situ* sequencing (ISS, N= 7 samples [4 reference, 3 DKD], 40551 glomerular cells).

Spatial mapping of glomerular cell types in diabetic kidney disease

To examine the glomerular milieu in DKD, we extracted podocytes, endothelial, and mesangial cells / VSMCs from the KPMP-HuBMAP snRNA-seq kidney atlas[14] (Figure 1A). Comparing healthy reference and DKD samples, expected pathways[23] were enriched in glomerular cell types (Figure 1B). For podocytes, enriched pathways included development and adhesion, sphingolipid metabolism, and VEGF signaling - all associated with mesangial expansion and neovascularization in DKD[27]. Endothelial cell pathways were enriched for proliferation and migration, consistent with the observed angiogenesis in DKD[28-30]. VSMC pathways aligned with the biological processes described above, including development, angiogenesis, and signaling. To quantitate cell type changes in DKD, we annotated glomeruli of ST samples histologically to differentiate glomerular and tubulointerstitial spots. Then, we deconvoluted the cell type composition of 1877 glomerular spots using a snRNAseq label transfer methodology[31] (Figure 1C). Across all glomeruli, the proportion of podocyte signature decreased in DKD with a concomitant increase in endothelial and VSMC signature relative to reference (Figure 1D). These changes are consistent with the podocyte effacement, neovascularization, and mesangial expansion often observed in DKD[9]. A similar cellular composition was observed with ISS, which confirmed upregulation of endothelial and mesangial cells within the diabetic glomeruli (Figure 1E).

Niche analysis uncovers a proliferative endothelial cell subtype

To define the spatial distribution of healthy and injured cell types as niches, we selected KPMP atlas-defined glomerular cell types including podocytes (POD), glomerular capillary endothelial cells (EC-GC), injured / degenerative Endothelial Cells (dEC), mesangial Cells (MC), injured / degenerative VSMCs (dVSMCs), other endothelial cells (now annotated as “not specified” or EC-NS) and other VSMCs (VSMC-NS) (Figure 2A). Expected marker gene expression was observed for POD, EC-GC, and MC, while injury genes were expressed in degenerative cell types (Figure 2B). Both EC-NS and VSMC-NS had reduced maker gene expression as compared to EC-GCs and MCs. Upon mapping these cell types onto glomerular spots, an increase in endothelial cell signature was observed in DKD, driven by increased EC-NS, rather than EC-GC or dEC signature (Figure 2C). Furthermore, EC-NS localized to glomerular spots proportionately more than TI spots. The glomerular mapping of the EC-NS and its proportional increase in DKD provided an impetus to identify an endothelial cell subtype, potentially associated with neovascularization.

To characterize colocalization niches, we clustered glomerular spots according to cell type composition (Supplemental Figure S1), identifying niches enriched in DKD or reference samples (Figure 2D). For example, a fibroblast-dominant niche (DKD Fib) was enriched in DKD. Three endothelial-dominant niches were identified, one in DKD (DKD EC) and two in reference (Ref EC 1, Ref EC 2). In the Ref EC 1 and 2 niches, EC-GC signature predominated, representing niches with healthy glomerular capillaries. In contrast, the DKD EC niche consisted of a high proportion of EC-NS. A differential expression analysis comparing DKD EC spots to Ref EC 1 and 2 spots identified genes associated with angiogenesis (*IGFBP7, CCN1, MT1G*), signaling (*TCIM, FRZB, SOST*), and injury (*MMP2, DEFB1*) (Figure 2E). We then back-mapped the expression signature of the three niches onto the snRNAseq and multiome atlases (Supplemental Figure S2) to identify the subcluster of EC-NS relevant to the DKD EC niche. The expression signature of this EC-NS subcluster is consistent with a unique DKD proliferative endothelial cell (prEC) phenotype (Figure 2F-G). The prEC could be further subtyped based on afferent arteriole (*PTGS1*), EC-GC (*MMP2*), and vasa recta (*ENPP2*) injury markers suggesting an anatomical trajectory embedded within this subtype (Supp. Figure 2). Differential expression between prECs and other endothelial cells in snRNAseq identified marker genes associated with angiogenesis (*SOX5, VEGFC, PALMD, ENPP2, MECOM, PDGFRB, JAG1), with the absence of known EC-GC (HECW2, TEK) and injury (ESRRG, SPP1)* markers (Figure 2H).

Anti-proliferative communication through SEMA6A and PLXNA2 is reduced in DKD

We sought to understand the cellular cross-talk underlying the changes in cell type proportion within DKD and reference niches. Using snRNAseq, we modelled communication between cell types with known receptor-ligand (RL) pairs in reference and DKD glomeruli (Figure 3, Supplemental Table S3). RL pairs associated with angiogenesis and cell proliferation were enriched in EC subtypes (Figure 3A). The *VEGFA–VEGFR* axis, a ligand-receptor pair vital to maintaining healthy glomerular vasculature[27], was present in both reference and DKD glomeruli. In contrast, the *SEMA6A-PLXNA2* RL pair, postulated to inhibit angiogenesis, was lost in certain endothelial cells of DKD. *SEMA6A* (Semaphorin 6a), expressed by endothelial cells, and *PLXNA2* (Plexin A2), expressed by both endothelial and VSMCs, are known to regulate cell adhesion[32], morphogenesis[33,34], and to modulate *VEGFA* signaling with an antiangiogenic effect[35,36]. Using ISS, we determined that glomerular expression density was reduced for *SEMA6A* (relative to *PECAM1*) and *PLXNA2* (relative to the sum of *PECAM1* and *TAGLN*) in DKD (Figure 3B).

To spatially contextualize these findings, we observed that *SEMA6A* and *PLXNA2* appropriately colocalize with *PECAM1* and *TAGLN*, in endothelial and VSMCs respectively (Figure 3C). *VEGFA* expression was maintained in reference and DKD samples (Figure 3D).

Other proangiogenic RL signaling was observed in DKD. Specifically, dECs expressed *VEGFA* in DKD, potentially contributing to EC proliferation. The prEC exhibited a pro-proliferative communication pattern with other endothelial cells in DKD through the RL pair *WNT2B-FZB4*[37,38] (Figure 3E). We found dysregulation of RL pairs involving fibronectin (*FN1*), with known involvement in wound healing and vascular development[39,40]. Finally, prECs also exhibited a unique communication pattern through the Notch (Figure 3F) pathway. The *DLL4*-Notch pair inhibits angiogenesis[41] and regulates proliferation and branching of new vessels[42]. prECs have reduced expression of the *DLL4* receptor in DKD, while *JAG1*/*JAG2*-Notch communication was maintained. Similar to the *VEGFA-VEGFRA* RL pair, angiopoetin-1 (*ANGPT1*) and TIE-2 (*TEK*) communication was maintained across all EC subtypes and in the MC and dVSMC. In contrast, other known RL pairs were dysregulated, including upregulation of platelet-derived growth factor-β (*PDGFB*) in prECs and its receptor (*PDGFRB*) in podocytes and all MC / VSMC subtypes. Likewise, transforming growth factor-β (*TGFB1*) signaling through its receptors (*TGFBR1, TGFBR2*) was upregulated in prECs and dVSMCs (Supplemental Table S3).

MEF2A, MEF2C, and TRPS1 control endothelial cell state transitions

We then leveraged a multiome dataset to define the regulatory networks underlying endothelial cell state transitions. Upon subsetting EC-GC and dEC cells (Figure 4A), we identified a trajectory emanating from the EC-GC (Figure 4B) and modeled the gene regulatory network (GRN) controlling this trajectory. The TFs *MEF2A, MEF2C,* and *TRPS1* present high centrality (Figure 4C) and are predicted to regulate *SEMA6A* and *PLXNA2* (Figure 4D). Within the multiome, we identified open chromatin peaks where these TFs are predicted to bind (Figures 4E-G) with reduced accessibility in dEC as compared to EC-GC. The mRNA expression is consistent with the accessibility. *MEF2A* and *MEF2C* are known to be involved in the maintenance of endothelial cell function and regulation of angiogenesis[43-47]. TRPS1 is implicated in angiogenic manifestations in tumors[48,49]. *MEF2A, MEF2C,* and *TRPS1* also regulated a trajectory for the EG-GC to prEC transition (Figure 4H-J), with the prEC marker gene, *PDGFB*, positively regulated by this TF network (Supplemental Figure S3)

Transcription factor knock-out disrupts endothelial cell trajectories

To evaluate the effect of *MEF2A, MEF2C,* and *TRPS1* in the glomerular endothelium, we performed *in silico* combined knock-out (KO) of the three TFs for two trajectories: EC-GC to either the dEC or prEC. CellOracle estimated the previously identified GRN in subclusters along the EC-GC to dEC trajectory (Figure 5A). The development flow of individual cells was qualitatively evaluated before and after KO (Figure 5B). The magnitude of developmental changes accelerated as assessed by the internal product of the two vectors in the force directed projection (Figure 5C) and along the pseudotime (Figure 5D). The KO resulted in a decrease of *SEMA6A, PLXNA2,* and *FZB4* in ECs. The individual KO of each TF was qualitatively similar (Supplemental Figure S4). For the EC-GC to prEC trajectory, the combined TF KO is shown to disrupt the trajectory, not accelerate it (Supplemental Figure S5). In summary, the *MEF2A, MEF2C,* and *TRPS1* TF network carefully balance the fate of the EC-GC. When the TF network is "on" or expressed, an EC-GC may progress to a prEC state. When the TF network is off, the EC-GC progresses toward an dEC or cell death state.

Vascular smooth muscle cell state transitions

A trajectory was identified from MC to VSMC-NS, ending in dVSMC (Supplemental Figure S6 A-B). In the GRN modelled for this trajectory, a TF of the myocyte enhancer factor 2 family, *MEF2D*, was identified to regulate the expression of its target gene *SMAD3* (Supplemental Figure S6 C). The chromatin accessibility in the predicted binding sites is consistent with the mRNA expression. *In silico* KO of this TF disrupted the trajectory directing the flow from MC and dVSMC to the VSMC-NS. (Supplemental Figure S6 D-G).

Histopathological associations with spatial niches and MEF2C activity

A pathologist scored each glomerulus using both images according to the categorial presence of histopathological features of hilar neovascularization, non-nodular mesangial sclerosis (mesangial expansion), nodular mesangial sclerosis (Kimmelstiel-Wilson nodule), and segmental glomerular sclerosis (SGS). To correlate our molecular findings, we performed ST in FFPE tissue. A trained pathologist scored the 7 µm thick H&E and 3 µm thick PAS sequential sections for each individual glomerulus for these features: hilar neovascularization, mesangial expansion, nodular mesangial sclerosis, and segmental glomerular sclerosis (SGS). We then merged the FFPE ST dataset and mapped onto it the niches previously identified. We observed that the endothelial DKD niche (DKD EC) had higher transfer scores than the Ref EC 2 in glomeruli with neovascularization (Figure 6A). The Ref EC 1 niche presented no mapping in FFPE tissue. The pro-fibrotic DKD FIB niche mapped to glomeruli with SGS lesions (Figure 6B).

MEF2C TF activity was inferred through expression of its target genes in the GRN. Estimated *MEF2C* activity localized over glomeruli and medullary rays in all samples (Figure 6C). However, *MEF2C* had increased activity in DKD glomerular spots. Within DKD glomeruli, *MEF2C* activity was associated with nodular mesangial sclerosis lesions (Figure 6D).

Spatial localization of EC and VSMC states

With ISS, we identified individual cells and localized the prEC phenotype to DKD glomeruli (Figure 6E). On reference we see the expected glomerular morphology. On a nodular DKD glomerulus, a relative loss of EC-GC was appreciated, with an increase in prEC quantity. In a second glomerulus, MCs transitioned to VSMC-NS, and finally stromal cells along the axis from hilum to nodule (Supplemental Figure S7). A small number of podocytes were seen in both DKD samples. We quantitated the prEC abundance relative to all other cells across each glomerulus in DKD and reference samples. The relative proportion of prECs increased 274.7 ± 1.8% ($p = 0.0015$) in DKD compared to reference (Figure 6F). Overall, this is consistent with the niches identified in ST. However, the cellular resolution suggests a morphological context to the changes observed in ST and the trajectories identified in multiome.

SGLT2i therapy reverses the dysregulation of MEF2C activity

To understand the impact of recent therapeutic advances on the *MEF2C* GRN, we accessed a human kidney scRNAseq dataset and assessed *MEF2C* target gene expression in EC-GCs of 3 conditions: healthy kidney, DKD without SGLT2i, and DKD with SGLT2i. In EC-GCs, 226 genes regulated by *MEF2C* were detected. In DKD, 66 genes were differentially expressed at $p < 0.05$ after Bonferroni correction (64 increased and 2 decreased expression) compared to individuals without DKD. SGLT2i therapy was associated with reversal toward a reference phenotype for 64 of these 66 dysregulated genes, including 43 at adjusted $p < 0.05$ (Figure 6G).

Discussion

In this work, we identified a unique niche, with dominant proliferative endothelial cell signature, that was associated with neovascularization in DKD. The niche was characterized by the loss of angiogenic inhibitory communication between the endothelial and VSMC. A TF network composed of *MEF2A, MEF2C,* and *TRPS1* regulated the transition between healthy canonical EC-GCs and proliferative (prEC) or degenerative (dEC) endothelial cell subtypes. *MEF2C* activity and prEC abundance were associated with histologic presence of nodular mesangial sclerosis and neovascularization.

Neovascularization is a complex phenomenon in DKD. It is currently unknown whether neovascularization represents an important adaptation or maladaptation. Glomerular hypertension in DKD may lead to localized hypoxia and sheer stress[50] and ultimately glomerulomegaly, an early adaptation to DKD, which is followed by subsequent fibrosis[51]. Hormone and cytokine signaling in DKD may protect from or contribute to neovascularization[52]. VEGF is required to maintain healthy EC-GC and mesangial cell functionality[10,11], but the balance of pro-angiogenic and inhibitory processes is tightly regulated. For example, angiopoetin-1 is pro-angiogenic and its interaction with Tie2 (*TEK*) also helps to establish and maintain healthy glomerular vascularity[53-55]. Similarly, *PDGFB-PDGFRB* signaling between endothelial and mesangial cells is required for appropriate formation of the capillary network within the glomerular tuft[56,57]. In contrast, the Notch pathway is well known to inhibit endothelial sprouting through its *DLL4* ligand interaction[42]; however, Jagged1 (*JAG1*) competes with *DLL4* to interact with Notch, restoring a pro-angiogenic state[41]. Consistent with this, in the KPMP dataset, we found maintenance of *ANGPT1-TEK, VEGFA-VEGFRA*, and *PDGFB-PDGFRB* RL pair pro-angiogenic signaling. *DLL4*-Notch signaling was lost in prECs of DKD subjects, but *JAG1*-Notch signaling was maintained. Traditionally, semaphorins and plexins have been described as contact inhibition proteins in axonogenesis[58,59]. These proteins have now been shown to be important in the inhibition of neovessel generation[59-61], but there is limited data in DKD. Our data support the contribution of *SEMA6A* and *PLXNA2* communication between the endothelial and mesangial cell population to maintain a healthy glomerular capillary structure. Our CellOracle KO of the TF network regulating *SEMA6A* and *PLXNA2* predicted a faster progression from an EC-GC to a degenerative endothelial cell and disrupted the transition to a proliferative endothelial cell.

Our rich dataset employed multiple orthogonal validations. Two disaggregated technologies, snRNAseq and multiome sequencing independently identified a similar set of endothelial subtypes. Likewise, we used three spatial technologies, Visium frozen which held the largest spot sample size, Visium FFPE with improved histologic morphometry, and Xenium which afforded single cell specificity in the histologic context. Combining all these technologies enhanced the confidence of the results. Although we focused our investigation on the glomerular cell cross-talk inherent in neovascularization and nodular mesangial sclerosis, we identified a broad set of molecular changes in DKD. There was substantial overlap in our molecular signature with prior seminal studies. When compared to an atlas of endothelial cell types, our ST glomeruli revealed the expected elevated expression of *PECAM1*, *GJA4*, and *NTN*, but minimal expression of the markers for other ECs[6]. For example, we identified upregulation of genes previously identified in DKD (*IGHM, COL1A2, CXCL6, COL6A3, MMP7*) in DKD glomeruli of the KPMP ST dataset[62]. Further, an analysis of cellular communication in glomerular hyperfiltration identified RL pairs such as *TGFB1*, *VEGFA*, *TGFBR2*, and *PDGFRB*[63], which aligned with signaling in the KPMP dataset. Thus, our study holds both internal and external validity. In addition, in a study of youth with Type 2 diabetes whose structural changes were limited to minor glomerulomegaly, SGLT2i therapy was associated with a robust reversal of the *MEF2C* activation signatures in glomerular endothelial cells, arguing for the plasticity and reversibility of the pathways described.

While glomeruli adapt to DKD through pro-angiogenic processes, the opposite phenomenon may be observed in the peritubular capillaries of the interstitium. Peritubular capillary rarefaction is a manifestation of chronic kidney disease[64]. The endothelial-to-mesenchymal transition underlying this rarefaction has substantial, but incomplete overlap with the signaling pathways observed in DKD glomeruli. For example, loss of Tie2 and VEGFA signaling accompany this mesenchymal transition. In murine models, conditional deletion of Twist (*Twist1*) and Snail (*Snai1*) both mitigated the endothelial-to-mesenchymal transition in peritubular capillaries. Soluble guanylate cyclase has been proposed as a potential therapeutic option to reduce endothelial dysfunction and prevent downstream proximal tubular epithelial-to-mesenchymal transition[65].

Our study interrogates the largest ST DKD sample size to date. Despite this, sample size remains a limitation as we were unable to subgroup subjects with DKD according to clinical features. To counterbalance this limitation, we conducted neighborhood analyses on a per spot level and histologic analyses on a per glomerular level to provide our study adequate power. A second limitation is the Visium ST spot size which overlies multiple cells. To overcome this, we included orthogonal validation with ISS, which allows for spatial resolution at the single cell level. Another significant strength of our study was the inclusion of histologic annotations for 74 glomeruli with an adjacent thin section. This strategy enabled us to link the molecular findings to histological features such as nodular mesangial sclerosis and hilar neovascularization.

In summary, we identified a novel proliferative endothelial cell subtype associated with neovascularization in DKD. A common challenge in snRNA-seq analysis is the insufficient power to determine whether two cell subtypes hold distinct biological relevance. Our strategy was to use spatially-defined niches to identify a biologically relevant proliferative endothelial cell cluster. This interrogation method may be applied to other tissues and conditions wherein cellular niches contribute to the molecular characteristics of a cell. Finally, we were able to identify changes in cell-cell communication and the regulatory network underlying the glomerular endothelial cell response to stress in DKD. Our data support that *MEF2C*, *MEF2A*, and *TRPS1* expression and regulation of *SEMA6A* and *PLXNA2* preserve the balance between endothelial cell proliferation and degeneration. In a human scRNAseq dataset, SGLT2i therapy restored the balance of *MEF2C* activity in EC-GCs of DKD towards the reference state in early stage disease suggesting that this pathway can be therapeutically targeted. Further studies are required to understand whether angiogenic processes in DKD are purely adaptive or whether therapies should be directed at limiting the extent of neovascularization.

Figure 1 - Glomerular cell types in diabetic kidney disease: **A)** A glomerular snRNAseq object was constructed with 16,488 nuclei representing cell types potentially localizing to glomeruli including all podocyte (POD), all endothelial cell (EC), and all vascular smooth muscle and mesangial cell (VSM/P) subtypes. **B)** Pathways enriched in the podocyte, VSM/P, and EC were determined for diabetic kidney disease (DKD, N=7) and reference (Ref) samples (N=18). **C)** Examples of Visium glomerular mapping of cell types in reference and DKD. An increased proportion of endothelial cell signature (orange) is observed in the diabetic glomerulus. Scale bar = 100 µm. **D)** The odds ratio of cell type signature vectors localized to glomeruli of reference and DKD samples in Visium ST (N=36). DKD glomeruli had reduced podocyte signature and increased EC signature as measured by Visium ST. For Xenium in situ sequencing (ISS, N=7), the number of cells of each cell type were localized to glomeruli of reference and DKD samples. VSM/P and EC cells were more abundant in DKD glomeruli, while podocytes were less frequent. **E)** An example of cell type mapping and segmentation with ISS, with expected markers defining each cell type. Pink – podocyte, Purple – VSM/P or mesangial cell, Orange – endothelial cell. Scale bar = 100 µm.

Figure 2 – Niche localization of proliferative endothelial cell subtype: **A-B)** Podocytes (POD), endothelial cells (EC) and vascular muscle cells (VSMC) were reclustered and annotated. Expression patterns within glomerular capillary endothelial cells (EC-GCs) and degenerative / injured endothelial cells (dEC) were compared to a composite cluster of all other endothelial cells (not specified or EC-NS). Mesangial cells (MCs), degenerative or injured VSMCs (dVSMC), and the remaining pool of vascular smooth muscle cells (VSMC-NS) were similarly compared. **C)** The glomerular mapping proportion from Visium ST according to condition (reference/Ref or diabetic kidney disease/DKD) and region (tubulointerstitium [TI] or glomerulus [glom]) revealed an increase in EC-NS signature in DKD glomeruli, suggesting an important unidentified glomerular cell type was embedded within the EC-NS cluster. Other cell types mapped to the appropriate region as expected (e.g. POD and MC in the glomerulus). **D)** All Visium glomerular ST spots (N= 1877) were clustered according to cell type vector proportion to define niches of colocalizing cells. Of the 21 identified niches, twelve were significantly enriched in either Ref or DKD samples, including a DKD EC niche with enrichment of EC-NS signature. **E)** Expression of selected genes differentially expressed between endothelial niches localizing to DKD or reference. **F-G)** The DKD EC niche signature was back-mapped into the glomerular snRNAseq and multiome object to identify a unique subcluster of endothelial cells defined by a proliferative or pro-angiogenic signature (prEC). **H)** Expression of selected genes differentially expressed in prEC in relation to other endothelial cells (prEC markers) in snRNAseq.

Figure 3 – Glomerular cell-cell communication: **A)** Angiogenesis-associated communication stemming from podocytes (POD) or endothelial cells (ECs). **B)** Transcript density of POD, EC, and mesangial cell (MC) markers from glomeruli of in situ sequencing samples. The density ratios of *SEMA6A* to *PECAM1* and *PLXNA2* to *PECAM1+TAGLN* were reduced in diabetic kidney disease (DKD). **C)** The colocalization of *SEMA1* (left) and *PLXNA2* (right) in a glomerulus. Blue arrowheads point to nuclei with colocalization of *PLXNA2* and either *PECAM1* or *TAGLN*. **D)** *VEGFA* expression localizing over glomeruli in a reference and DKD sample. **E)** Angiogenesis-associated communication stemming from proliferative endothelial cells (prECs). **F)** Jag-Notch and *DLL4*-Notch communication involving proliferative endothelial cells. Glomerular capillary endothelial cells: EC-GC; degenerative endothelial cell: dEC; proliferative Endothelial cell: prEC; endothelial not specified (without prEC): EC-NS; mesangial cells: MC, degenerative vascular smooth muscle cell (dVSMC); VSMC not specified: VSMC-NS.

Figure 4 – Transcription factor regulation of endothelial cell trajectories: **A)** Force directed projection of Endothelial Cell Glomerular Capillaries and degenerative endothelial cells (dEC). **B)** Pseudotime trajectory from EC-GC to dEC. **C)** Out influence centrality measure of the gene regulatory network associated with the EC-GC to dEC trajectory identifies

MEF2A, *MEF2C*, and *TRPS1* as a transcription factor network. **D)** *MEF2A*, *MEF2C*, and *TRPS1* regulate *SEMA6A* and *PLXNA2* (number of peaks regulated is stated next to arrows). **E)** Chromatin accessibility tracks of *SEMA6A* for glomerular cell types with predicted accessible binding sites of *MEF2A*, *MEF2C*, and *TRPS1*. **F)** Chromatin accessibility tracks of *MEF2C* for glomerular cell types with predicted accessible binding sites of *MEF2C* and *TRPS1*. **G)** Chromatin accessibility tracks of *PLXNA2* for glomerular cell types with predicted accessible binding sites of *MEF2A* and *MEF2C*. **H)** Force directed projection of Endothelial Cell Glomerular Capillaries and proliferative endothelial cells (prEC). **I)** Pseudotime trajectory from EC-GC to prEC. **J)** Out influence centrality measure suggests the same gene regulatory network controls the EC-GC to prEC trajectory.

Figure 5 – Combined *in silico* knockout: **A)** CellOracle modeled subclusters in the EC-GC to dEC trajectory. **B)** Development flow (left) is accelerated after knockout (right). **C)** Internal product between developmental fields before and after knockout shows acceleration throughout the EC-GC transition to dEC after knockout. **D)** Internal product between developmental fields along the pseudotime. **E)** Expression of transcription factor and target genes before and after knockout reveal reduction of *SEMA6A* and *PLXNA2* after knockout.

Figure 6 – Histopathological and morphological associations with molecular data: **A)** The diabetic kidney disease (DKD) endothelial cell (EC) niche was associated with the presence of histologic neovascularization in glomeruli of FFPE samples. Arrows identify an example of neovascularization near a glomerular hilum. * = $p < 0.001$. **B)** The DKD fibroblast (FIB) niche was associated with focal segmental glomerulosclerosis (FSGS) lesions in glomeruli of FFPE samples. The arrowhead points to an area of segmental sclerosis as an example. * = $p < 0.03$. **C)** Transfer score mapping of *MEF2C* activity on FFPE samples reveals localization mainly to glomeruli (but also medullary rays). MEF2C activity was estimated from a vector of composite target gene expression. **D)** *MEF2C* activity was increased in DKD glomeruli and further increased in those with nodular mesangial sclerosis (KW nodules). *= $p < 0.01$. Ref = reference; DKD N = DKD glomerulus without the histologic feature; DKD Y = DKD glomerulus with the histologic feature. **E)** Example of a reference glomerulus and a DKD glomerulus with neovascularization and nodular mesangial sclerosis with individual cell types annotated. **F)** Ratio of prEC to EC-GC per glomeruli across Ref and DKD samples. * = $p < 0.015$. **G)** The fold change of selected *MEF2C* targeted genes is altered in DKD and restored after sodium glucose transporter-2 therapy (SGLT2i).

Supplemental Figure S1 – Niche clustering: **A)** UMAP projection presenting the spots clustering in the identified niches from Visium ST. Each dot represents one niche or ST spot. Spots were clustered according to Seurat cell type transfer scores. **B)** Breakdown of spots by condition in the UMAP projection. Ref = reference, DKD = diabetic kidney disease. **C)** The odds ratio of each of the 21 niches identified based on their likelihood of localizing to DKD glomeruli v reference glomeruli. **D)** Average cell type proportion of each niche.

Supplemental Figure S2 – Mapping of endothelial niches: **A)** Mapping of endothelial niches onto the multiome dataset. **B)** Multiome cluster with prevalent mapping of diabetic kidney disease endothelial (DKD EC) niche annotated as a proliferative endothelial subcluster (prEC). **C)** Expression of selected genes along the multiome prEC cluster. **D)** Mapping of endothelial niches onto the snRNAseq dataset. **E)** snRNAseq cluster with prevalent mapping of the DKD EC niche annotated as a prEC subcluster. **F)** Expression of selected genes along the snRNAseq prEC cluster.

Supplemental Figure S3 - Regulation of *PDGFB* and prEC marker genes: **A)** Marker genes of prEC (Repeated from Figure 2 for direct comparison with panel C). **B)** Accessibility tracks for *PDGFB* from multiome. All highlighted peaks are predicted to be regulated by *MEF2A* and *MEF2C*. **C)** Logarithm of the Fold Change in expression of prEC marker genes after the combined knock out of *MEF2A*, *MEF2C* and *TRPS1* relative to original expression. **D)** Expression of select genes before and after knock out. **E)** Transcript density in ISS of *PDGFRB* in glomeruli. **F)** Localization in ISS of *PDGFRB* in a Reference and a DKD glomeruli.

Supplemental Figure S4 – Development flow disrupted by individual *in silico* knock out of: **A)** *MEF2A*, **B)** *MEF2D*, and **C)** *TRPS1* in the EC-GC to dEC trajectory.

Supplemental Figure S5 – Combined *In silico* knock out of the EC-GC to prEC trajectory: **A)** CellOracle modeled subclusters in the EC-GC to prEC trajectory. **B)** Development flow (left) is disrupted after knockout of *MEF2A*, *MEF2C*, and *TRPS1* (right). **C)** Internal product between developmental fields before and after knockout. **D)** Internal product between developmental fields along pseudotime. **E)** Expression of transcription factor and target genes before and after knockout.

Supplemental Figure S6 – Multiome analysis of mesangial and vascular smooth muscle cells: **A)** Force directed projection of mesangial and vascular smooth muscle cells. **B)** Pseudotime trajectory from MC to dVSMC. **C)** Chromatin accessibility tracks of *SMAD3* for glomerular cell types with predicted accessible binding sites of *MEF2D*. **D)** CellOracle modeled subclusters in the MC to dVSMC trajectory. **E)** Development flow (left) is disrupted after knockout of *MEF2D* (right). **E)** Internal product between developmental fields before and after knockout. **G)** Internal product between developmental fields along pseudotime.

Supplemental Figure S7 – Example of a DKD glomerulus in ISS. **A)** Example o DKD glomerulus with hilar neovascularization and segmental glomerular sclerosis.

Abbreviations: KPMP; HuBMAP; snRNAseq; ST; ISS; snRNA-seq; sc/snRNA-seq; OCT; FFPE; H&E; PAS;

ACKNOWLEDGMENTS

RMF was supported by a Paul Teschan Research fund Project NO 2023-01 from Dialysis Clinic, Inc. MTE was supported by R01AT011463, R01DK114485, U54 DK134301-01, and U01DK114923. PS was supported by R01DK114485. We would like to acknowledge the NIH common fund Human Biomolecular Atlas Project (HuBMAP) and the NIDDK's Kidney Precision Medicine Project. This research was supported in part by the Indiana University Pervasive Technology Institute and the Washington University Kidney Translational Research Center. The KPMP is funded by the following grants from the NIDDK: U01DK133081, U01DK133091, U01DK133092, U01DK133093, U01DK133095, U01DK133097, U01DK114866, U01DK114908, U01DK133090, U01DK133113, U01DK133766, U01DK133768, U01DK114907, U01DK114920, U01DK114923, U01DK114933, U24DK114886.

AUTHOR CONTRIBUTIONS:

MTE, RMF, CEA: Conceptualization; SJ, KJK, SER, JRS, RDT: Specimen acquisition; MTE, SJ, RMF, YHC, DLG, CLP, BBL, WSB, FF, MA, AS, DB, MJF, JAS, VN, MK: Data generation; YHC, RMF, DLG, DB: Data curation; RMF, DLG, VN, MTE: Formal analysis; MTE, SJ, PCD, TME, JH, MK: Funding acquisition; All authors: Investigation; All authors: Methodology; RMF: Project administration; RMF, MTE: Writing - original draft; All authors: Writing - review & editing. KPMP: provision of infrastructure.

Please address data and materials requests for Xenium or Visium data to Michael Eadon (meadon@iu.edu),

COMPETING INTERESTS

The authors have nothing to disclose.

DATA AVAILABILITY

snRNAseq data was obtained from the KPMP – HuBMAP kidney atlas[14].Multiome is a published KPMP – HuBMAP dataset[17]. Both datasets, along with the Visium samples, are available on KPMP atlas repository. Code to reproduce analysis can be found on https://github.com/rimelof/Melo_Ferreira_et_al._neovascularization_2024

References:

1. Johansen KL, Gilbertson DT, Li S, et al. US Renal Data System 2023 Annual Data Report: Epidemiology of Kidney Disease in the United States. *Am J Kidney Dis*. Apr 2024;83(4S1):A8-A13. doi:10.1053/j.ajkd.2024.01.001
2. Olson JL, Heptinstall RH. Nonimmunologic mechanisms of glomerular injury. *Lab Invest*. Nov 1988;59(5):564-578.
3. Najafian B, Alpers CE, Fogo AB. Pathology of human diabetic nephropathy. *Contrib Nephrol*. 2011;170:36-47. doi:10.1159/000324942
4. Dai H, Liu Q, Liu B. Research Progress on Mechanism of Podocyte Depletion in Diabetic Nephropathy. *J Diabetes Res*. 2017;2017:2615286. doi:10.1155/2017/2615286
5. Dimke H, Maezawa Y, Quaggin SE. Crosstalk in glomerular injury and repair. *Curr Opin Nephrol Hypertens*. May 2015;24(3):231-238. doi:10.1097/MNH.0000000000000117
6. Zhang K, Kan H, Mao A, et al. Integrated Single-Cell Transcriptomic Atlas of Human Kidney Endothelial Cells. *J Am Soc Nephrol*. May 1 2024;35(5):578-593. doi:10.1681/ASN.0000000000000320
7. Wahab NA, Schaefer L, Weston BS, et al. Glomerular expression of thrombospondin-1, transforming growth factor beta and connective tissue growth factor at different stages of diabetic nephropathy and their interdependent roles in mesangial response to diabetic stimuli. *Diabetologia*. Dec 2005;48(12):2650-2660. doi:10.1007/s00125-005-0006-5
8. Jain S, Eadon MT. Spatial transcriptomics in health and disease. *Nat Rev Nephrol*. May 8 2024;doi:10.1038/s41581-024-00841-1
9. Fogo AB. Glomerular hypertension, abnormal glomerular growth, and progression of renal diseases. *Kidney Int Suppl*. Apr 2000;75:S15-21.
10. Sivaskandarajah GA, Jeansson M, Maezawa Y, Eremina V, Baelde HJ, Quaggin SE. Vegfa protects the glomerular microvasculature in diabetes. *Diabetes*. Nov 2012;61(11):2958-2966. doi:10.2337/db11-1655
11. Eremina V, Cui S, Gerber H, et al. Vascular endothelial growth factor a signaling in the podocyte-endothelial compartment is required for mesangial cell migration and survival. *J Am Soc Nephrol*. Mar 2006;17(3):724-735. doi:10.1681/ASN.2005080810
12. Cooper M, Cherney DZI, Greene TH, et al. Vascular Endothelial Growth Factor-B Blockade with CSL346 in Diabetic Kidney Disease: A Phase 2A Randomized Controlled Trial. *J Am Soc Nephrol*. Aug 16 2024;doi:10.1681/ASN.0000000000000438
13. Ferkowicz MJ, Verma A, Barwinska D, et al. Molecular Signatures of Glomerular Neovascularization in a Patient with Diabetic Kidney Disease. *Clin J Am Soc Nephrol*. Aug 3 2023;19(2):266-275. doi:10.2215/CJN.0000000000000276
14. Lake BB, Menon R, Winfree S, et al. An atlas of healthy and injured cell states and niches in the human kidney. *Nature*. Jul 2023;619(7970):585-594. doi:10.1038/s41586-023-05769-3
15. Melo Ferreira R, Sabo AR, Winfree S, et al. Integration of spatial and single-cell transcriptomics localizes epithelial cell-immune cross-talk in kidney injury. *JCI Insight*. Jun 22 2021;6(12)doi:10.1172/jci.insight.147703
16. Melo Ferreira R, Freije BJ, Eadon MT. Deconvolution Tactics and Normalization in Renal Spatial Transcriptomics. *Front Physiol*. 2021;12:812947. doi:10.3389/fphys.2021.812947
17. Gisch DL, Brennan M, Lake BB, et al. The chromatin landscape of healthy and injured cell types in the human kidney. *Nat Commun*. Jan 10 2024;15(1):433. doi:10.1038/s41467-023-44467-6
18. Eadon MT, Schwantes-An TH, Phillips CL, et al. Kidney Histopathology and Prediction of Kidney Failure: A Retrospective Cohort Study. *Am J Kidney Dis*. Sep 2020;76(3):350-360. doi:10.1053/j.ajkd.2019.12.014
19. Michael Eadon RMF, Ying-Hua Cheng, Tarek M. El-Achkar Spatial Transcriptomics Protocol. 2021
20. Korsunsky I, Millard N, Fan J, et al. Fast, sensitive and accurate integration of single-cell data with Harmony. *Nat Methods*. Dec 2019;16(12):1289-1296. doi:10.1038/s41592-019-0619-0
21. Jin S, Plikus MV, Nie Q. CellChat for systematic analysis of cell-cell communication from single-cell and spatially resolved transcriptomics. *bioRxiv*. 2023:2023.2011.2005.565674. doi:10.1101/2023.11.05.565674
22. Hao Y, Hao S, Andersen-Nissen E, et al. Integrated analysis of multimodal single-cell data. *Cell*. Jun 24 2021;184(13):3573-3587 e3529. doi:10.1016/j.cell.2021.04.048
23. Bibby JA, Agarwal D, Freiwald T, et al. Systematic single-cell pathway analysis to characterize early T cell activation. *Cell Rep*. Nov 22 2022;41(8):111697. doi:10.1016/j.celrep.2022.111697
24. Li Z, Nagai JS, Kuppe C, Kramann R, Costa IG. scMEGA: single-cell multi-omic enhancer-based gene regulatory network inference. *Bioinform Adv*. 2023;3(1):vbad003. doi:10.1093/bioadv/vbad003

25. Kamimoto K, Stringa B, Hoffmann CM, Jindal K, Solnica-Krezel L, Morris SA. Dissecting cell identity via network inference and in silico gene perturbation. *Nature*. Feb 2023;614(7949):742-751. doi:10.1038/s41586-022-05688-9

26. Schaub JA, AlAkwaa FM, McCown PJ, et al. SGLT2 inhibitors mitigate kidney tubular metabolic and mTORC1 perturbations in youth-onset type 2 diabetes. *J Clin Invest*. Mar 1 2023;133(5)doi:10.1172/JCI164486

27. Kanesaki Y, Suzuki D, Uehara G, et al. Vascular endothelial growth factor gene expression is correlated with glomerular neovascularization in human diabetic nephropathy. *Am J Kidney Dis*. Feb 2005;45(2):288-294. doi:10.1053/j.ajkd.2004.09.020

28. Min W, Yamanaka N. Three-dimensional analysis of increased vasculature around the glomerular vascular pole in diabetic nephropathy. *Virchows Arch A Pathol Anat Histopathol*. 1993;423(3):201-207. doi:10.1007/BF01614771

29. Osterby R, Asplund J, Bangstad HJ, et al. Neovascularization at the vascular pole region in diabetic glomerulopathy. *Nephrol Dial Transplant*. Feb 1999;14(2):348-352. doi:10.1093/ndt/14.2.348

30. Cossey LN, Hennigar RA, Bonsib S, Gown AM, Silva FG. Vascular mesangial channels in human nodular diabetic glomerulopathy. *Hum Pathol*. Feb 2016;48:148-153. doi:10.1016/j.humpath.2015.09.018

31. Stuart T, Butler A, Hoffman P, et al. Comprehensive Integration of Single-Cell Data. *Cell*. Jun 13 2019;177(7):1888-1902.e1821. doi:10.1016/j.cell.2019.05.031

32. Ebert AM, Childs SJ, Hehr CL, Cechmanek PB, McFarlane S. Sema6a and Plxna2 mediate spatially regulated repulsion within the developing eye to promote eye vesicle cohesion. *Development*. Jun 2014;141(12):2473-2482. doi:10.1242/dev.103499

33. Belle M, Parray A, Belle M, Chedotal A, Nguyen-Ba-Charvet KT. PlexinA2 and Sema6A are required for retinal progenitor cell migration. *Dev Growth Differ*. Jun 2016;58(5):492-502. doi:10.1111/dgd.12298

34. Perez-Branguli F, Zagar Y, Shanley DK, Graef IA, Chedotal A, Mitchell KJ. Reverse Signaling by Semaphorin-6A Regulates Cellular Aggregation and Neuronal Morphology. *PLoS One*. 2016;11(7):e0158686. doi:10.1371/journal.pone.0158686

35. Segarra M, Ohnuki H, Maric D, et al. Semaphorin 6A regulates angiogenesis by modulating VEGF signaling. *Blood*. Nov 8 2012;120(19):4104-4115. doi:10.1182/blood-2012-02-410076

36. Dhanabal M, Wu F, Alvarez E, et al. Recombinant semaphorin 6A-1 ectodomain inhibits in vivo growth factor and tumor cell line-induced angiogenesis. *Cancer Biol Ther*. Jun 2005;4(6):659-668. doi:10.4161/cbt.4.6.1733

37. Zhao X, Zhang Z, Zhu Q, et al. Modeling human ectopic pregnancies with trophoblast and vascular organoids. *Cell Rep*. Jun 27 2023;42(6):112546. doi:10.1016/j.celrep.2023.112546

38. Miao Y, Tan C, Pek NM, et al. Deciphering Endothelial and Mesenchymal Organ Specification in Vascularized Lung and Intestinal Organoids. *bioRxiv*. Feb 7 2024;doi:10.1101/2024.02.06.577460

39. Schwarzbauer JE, DeSimone DW. Fibronectins, their fibrillogenesis, and in vivo functions. *Cold Spring Harb Perspect Biol*. Jul 1 2011;3(7)doi:10.1101/cshperspect.a005041

40. Chiang HY, Korshunov VA, Serour A, Shi F, Sottile J. Fibronectin is an important regulator of flow-induced vascular remodeling. *Arterioscler Thromb Vasc Biol*. Jul 2009;29(7):1074-1079. doi:10.1161/ATVBAHA.108.181081

41. Benedito R, Roca C, Sorensen I, et al. The notch ligands Dll4 and Jagged1 have opposing effects on angiogenesis. *Cell*. Jun 12 2009;137(6):1124-1135. doi:10.1016/j.cell.2009.03.025

42. Pitulescu ME, Schmidt I, Giaimo BD, et al. Dll4 and Notch signalling couples sprouting angiogenesis and artery formation. *Nat Cell Biol*. Aug 2017;19(8):915-927. doi:10.1038/ncb3555

43. Liu B, Wang L, Jiang W, et al. Myocyte enhancer factor 2A delays vascular endothelial cell senescence by activating the PI3K/p-Akt/SIRT1 pathway. *Aging (Albany NY)*. Jun 10 2019;11(11):3768-3784. doi:10.18632/aging.102015

44. Li T, Conroy KL, Kim AM, et al. Role of MEF2C in the Endothelial Cells Derived from Human Induced Pluripotent Stem Cells. *Stem Cells*. Apr 25 2023;41(4):341-353. doi:10.1093/stmcls/sxad005

45. Xu Z, Yoshida T, Wu L, Maiti D, Cebotaru L, Duh EJ. Transcription factor MEF2C suppresses endothelial cell inflammation via regulation of NF-kappaB and KLF2. *J Cell Physiol*. Jun 2015;230(6):1310-1320. doi:10.1002/jcp.24870

46. Xu Z, Gong J, Maiti D, et al. MEF2C ablation in endothelial cells reduces retinal vessel loss and suppresses pathologic retinal neovascularization in oxygen-induced retinopathy. *Am J Pathol*. Jun 2012;180(6):2548-2560. doi:10.1016/j.ajpath.2012.02.021

47. Sturtzel C, Testori J, Schweighofer B, Bilban M, Hofer E. The transcription factor MEF2C negatively controls angiogenic sprouting of endothelial cells depending on oxygen. *PLoS One*. 2014;9(7):e101521. doi:10.1371/journal.pone.0101521

48. Wu M, Sun X, Wang T, Zhang M, Li P. TRPS1 knockdown inhibits angiogenic vascular mimicry in human triple negative breast cancer cells. *Clin Transl Oncol*. Jan 2022;24(1):145-153. doi:10.1007/s12094-021-02676-9

49. Li Z, Jia M, Wu X, Cui J, Pan A, Li L. Overexpression of Trps1 contributes to tumor angiogenesis and poor prognosis of human osteosarcoma. *Diagn Pathol*. Sep 17 2015;10:167. doi:10.1186/s13000-015-0401-2
50. Yoshida Y, Fogo A, Ichikawa I. Glomerular hemodynamic changes vs. hypertrophy in experimental glomerular sclerosis. *Kidney Int*. Feb 1989;35(2):654-660. doi:10.1038/ki.1989.35
51. Ichikawa I, Ikoma M, Fogo A. Glomerular growth promoters, the common key mediator for progressive glomerular sclerosis in chronic renal diseases. *Adv Nephrol Necker Hosp*. 1991;20:127-148.
52. Bartlett CS, Jeansson M, Quaggin SE. Vascular Growth Factors and Glomerular Disease. *Annu Rev Physiol*. 2016;78:437-461. doi:10.1146/annurev-physiol-021115-105412
53. Liu J, Nair V, Zhao YY, et al. Multi-Scalar Data Integration Links Glomerular Angiopoietin-Tie Signaling Pathway Activation With Progression of Diabetic Kidney Disease. *Diabetes*. Dec 1 2022;71(12):2664-2676. doi:10.2337/db22-0169
54. Li Y, Liu P, Zhou Y, et al. Activation of Angiopoietin-Tie2 Signaling Protects the Kidney from Ischemic Injury by Modulation of Endothelial-Specific Pathways. *J Am Soc Nephrol*. Jun 1 2023;34(6):969-987. doi:10.1681/ASN.0000000000000098
55. Carota IA, Kenig-Kozlovsky Y, Onay T, et al. Targeting VE-PTP phosphatase protects the kidney from diabetic injury. *J Exp Med*. Apr 1 2019;216(4):936-949. doi:10.1084/jem.20180009
56. Lindahl P, Hellstrom M, Kalen M, et al. Paracrine PDGF-B/PDGF-Rbeta signaling controls mesangial cell development in kidney glomeruli. *Development*. Sep 1998;125(17):3313-3322. doi:10.1242/dev.125.17.3313
57. Bjarnegard M, Enge M, Norlin J, et al. Endothelium-specific ablation of PDGFB leads to pericyte loss and glomerular, cardiac and placental abnormalities. *Development*. Apr 2004;131(8):1847-1857. doi:10.1242/dev.01080
58. Nourisanami F, Sobol M, Li Z, et al. Molecular mechanisms of proteoglycan-mediated semaphorin signaling in axon guidance. *Proc Natl Acad Sci U S A*. Jul 30 2024;121(31):e2402755121. doi:10.1073/pnas.2402755121
59. Bhat GP, Maurizio A, Motta A, et al. Structured wound angiogenesis instructs mesenchymal barrier compartments in the regenerating nerve. *Neuron*. Jan 17 2024;112(2):209-229 e211. doi:10.1016/j.neuron.2023.10.025
60. Sakurai A, Gavard J, Annas-Linhares Y, et al. Semaphorin 3E initiates antiangiogenic signaling through plexin D1 by regulating Arf6 and R-Ras. *Mol Cell Biol*. Jun 2010;30(12):3086-3098. doi:10.1128/MCB.01652-09
61. Sabag AD, Smolkin T, Mumblat Y, et al. The role of the plexin-A2 receptor in Sema3A and Sema3B signal transduction. *J Cell Sci*. Dec 15 2014;127(Pt 24):5240-5252. doi:10.1242/jcs.155960
62. Woroniecka KI, Park AS, Mohtat D, Thomas DB, Pullman JM, Susztak K. Transcriptome analysis of human diabetic kidney disease. *Diabetes*. Sep 2011;60(9):2354-2369. doi:10.2337/db10-1181
63. Stefansson VTN, Nair V, Melsom T, et al. Molecular programs associated with glomerular hyperfiltration in early diabetic kidney disease. *Kidney Int*. Dec 2022;102(6):1345-1358. doi:10.1016/j.kint.2022.07.033
64. Lovisa S, Fletcher-Sananikone E, Sugimoto H, et al. Endothelial-to-mesenchymal transition compromises vascular integrity to induce Myc-mediated metabolic reprogramming in kidney fibrosis. *Sci Signal*. Jun 9 2020;13(635)doi:10.1126/scisignal.aaz2597
65. Balzer MS, Pavkovic M, Frederick J, et al. Treatment effects of soluble guanylate cyclase modulation on diabetic kidney disease at single-cell resolution. *Cell Rep Med*. Apr 18 2023;4(4):100992. doi:10.1016/j.xcrm.2023.100992

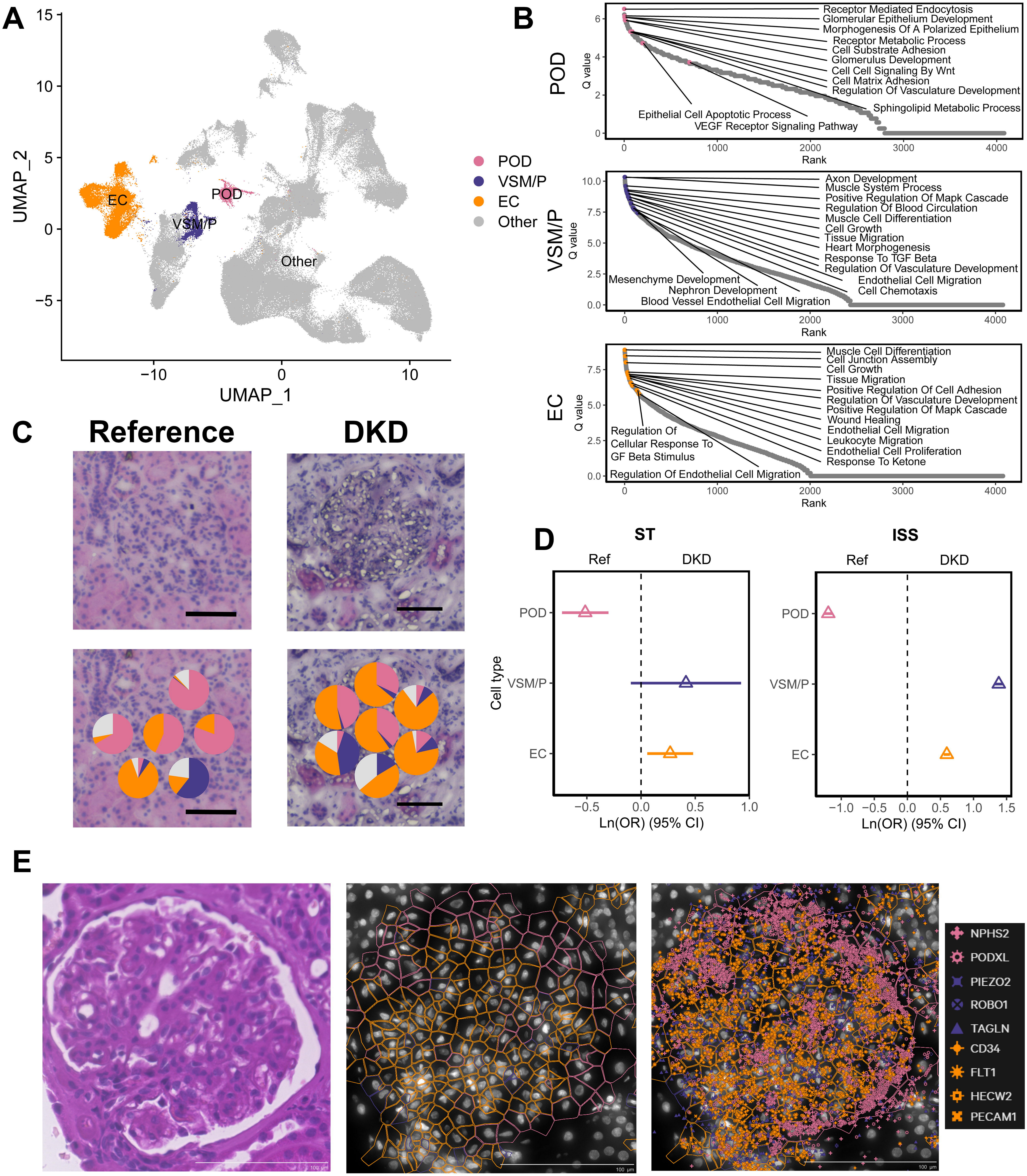
A
B
C
D
E
UMAP_1
UMAP_2
EC
VSM/P
POD
Other
POD
VSM/P
EC
Other
POD
Q value
Rank
Receptor Mediated Endocytosis
Glomerular Epithelium Development
Morphogenesis Of A Polarized Epithelium
Receptor Metabolic Process
Cell Substrate Adhesion
Glomerulus Development
Cell Cell Signaling By Wnt
Cell Matrix Adhesion
Regulation Of Vasculature Development
Sphingolipid Metabolic Process
Epithelial Cell Apoptotic Process
VEGF Receptor Signaling Pathway
VSM/P
Axon Development
Muscle System Process
Positive Regulation Of Mapk Cascade
Regulation Of Blood Circulation
Muscle Cell Differentiation
Cell Growth
Tissue Migration
Heart Morphogenesis
Response To TGF Beta
Regulation Of Vasculature Development
Endothelial Cell Migration
Cell Chemotaxis
Mesenchyme Development
Nephron Development
Blood Vessel Endothelial Cell Migration
EC
Muscle Cell Differentiation
Cell Junction Assembly
Cell Growth
Tissue Migration
Positive Regulation Of Cell Adhesion
Regulation Of Vasculature Development
Positive Regulation Of Mapk Cascade
Wound Healing
Endothelial Cell Migration
Leukocyte Migration
Endothelial Cell Proliferation
Response To Ketone
Regulation Of Cellular Response To GF Beta Stimulus
Regulation Of Endothelial Cell Migration
Reference
DKD
ST
ISS
Ref
DKD
Cell type
POD
VSM/P
EC
Ln(OR) (95% CI)
NPHS2
PODXL
PIEZO2
ROBO1
TAGLN
CD34
FLT1
HECW2
PECAM1
100 µm

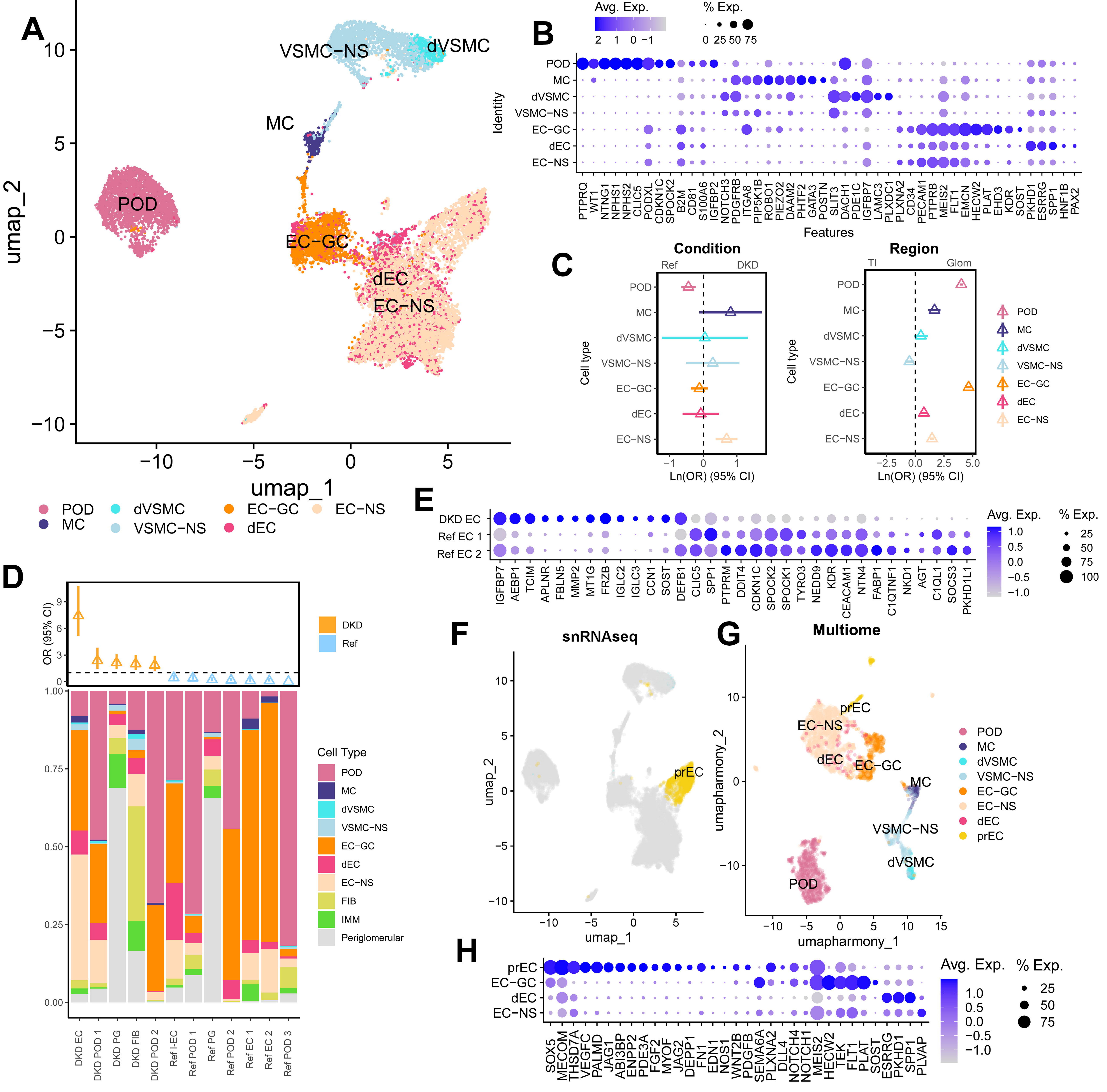
A
umap_2
umap_1
POD
MC
VSMC−NS
dVSMC
EC−GC
dEC
EC−NS
B
Avg. Exp.
% Exp.
Identity
Features
PTPRQ WT1 NTNG1 NPHS1 NPHS2 CLIC5 PODXL CDKN1C SPOCK2 B2M CD81 S100A6 IGFBP2 NOTCH3 PDGFRB ITGA8 PIP5K1B ROBO1 PIEZO2 DAAM2 PHTF2 GATA3 POSTN SLIT3 DACH1 PDE1C IGFBP7 LAMC3 PLXDC1 PLXNA2 CD34 PECAM1 PTPRB MEIS2 FLT1 EMCN HECW2 PLAT EHD3 KDR SOST PKHD1 ESRRG SPP1 HNF1B PAX2
C
Condition
Ref
DKD
Region
TI
Glom
Cell type
Ln(OR) (95% CI)
D
OR (95% CI)
DKD
Ref
Cell Type
POD
MC
dVSMC
VSMC−NS
EC−GC
dEC
EC−NS
FIB
IMM
Periglomerular
DKD EC
DKD POD 1
DKD PG
DKD FIB
DKD POD 2
Ref I-EC
Ref POD 1
Ref PG
Ref POD 2
Ref EC 1
Ref EC 2
Ref POD 3
E
DKD EC
Ref EC 1
Ref EC 2
IGFBP7 AEBP1 TCIM APLNR FBLN5 MMP2 MT1G FRZB IGLC2 IGLC3 CCN1 SOST DEFB1 CLIC5 SPP1 PTPRM DDIT4 CDKN1C SPOCK2 SPOCK1 TYRO3 NEDD9 KDR CEACAM1 NTN4 FABP1 C1QTNF1 NKD1 AGT C1QL1 SOCS3 PKHD1L1
F
snRNAseq
prEC
umap_1
umap_2
G
Multiome
prEC
umapharmony_1
umapharmony_2
H
prEC
EC−GC
dEC
EC−NS
SOX5 MECOM THSD7A VEGFC PALMD JAG1 ABI3BP ENPP2 PDE3A FGF2 MYOF JAG2 DEPP1 FN1 EDN1 NOS1 WNT2B PDGFB SEMA6A PLXNA2 DLL4 NOTCH4 NOTCH1 MEIS2 HECW2 TEK FLT1 PLAT SOST ESRRG PKHD1 SPP1 PLVAP

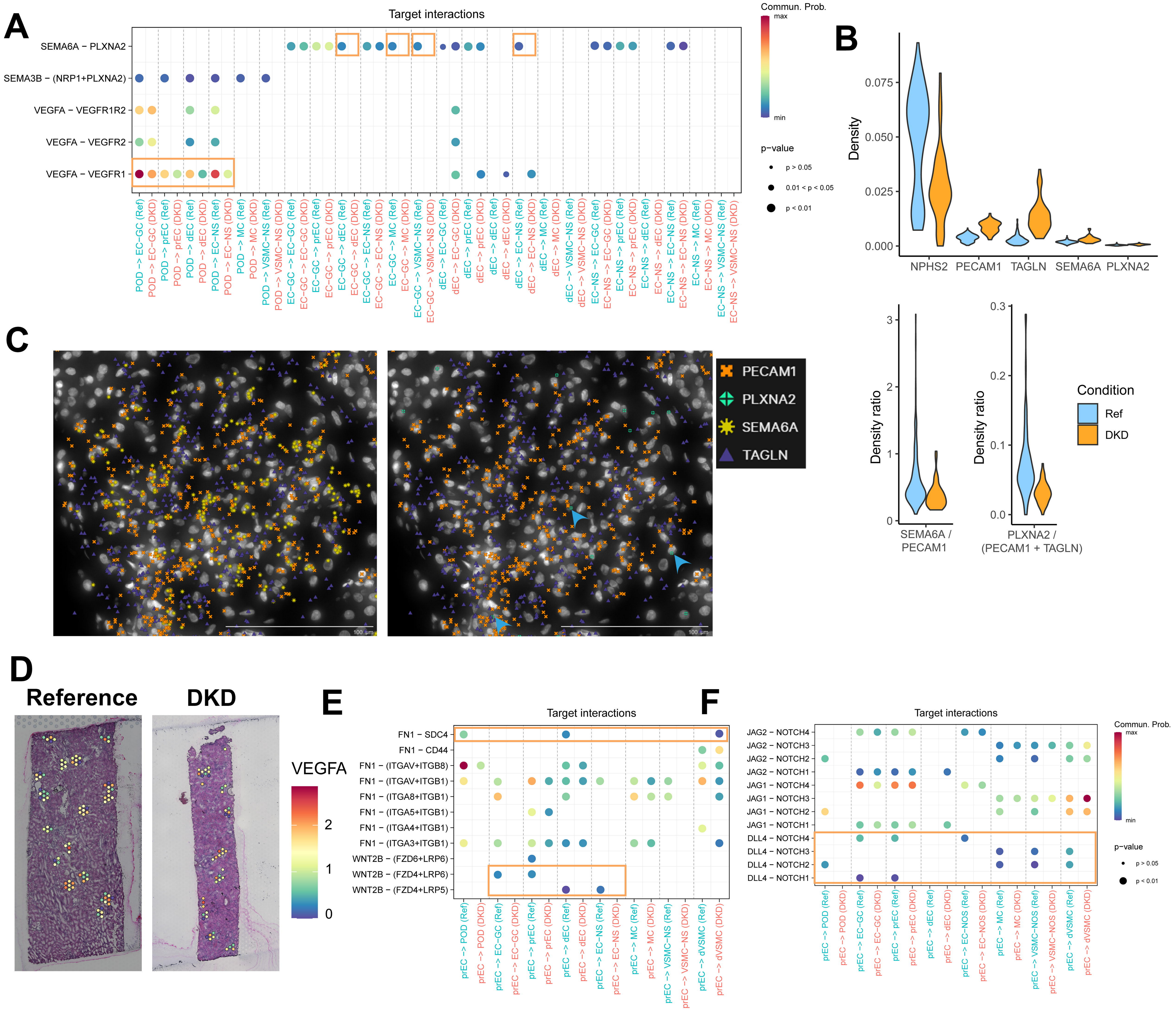
A
Target interactions
SEMA6A - PLXNA2
SEMA3B - (NRP1+PLXNA2)
VEGFA - VEGFR1R2
VEGFA - VEGFR2
VEGFA - VEGFR1
POD -> EC-GC (Ref)
POD -> EC-GC (DKD)
POD -> prEC (Ref)
POD -> prEC (DKD)
POD -> dEC (Ref)
POD -> dEC (DKD)
POD -> EC-NS (Ref)
POD -> EC-NS (DKD)
POD -> MC (Ref)
POD -> MC (DKD)
POD -> VSMC-NS (Ref)
POD -> VSMC-NS (DKD)
EC-GC -> EC-GC (Ref)
EC-GC -> EC-GC (DKD)
EC-GC -> prEC (Ref)
EC-GC -> prEC (DKD)
EC-GC -> dEC (Ref)
EC-GC -> dEC (DKD)
EC-GC -> EC-NS (Ref)
EC-GC -> EC-NS (DKD)
EC-GC -> MC (Ref)
EC-GC -> MC (DKD)
EC-GC -> VSMC-NS (Ref)
EC-GC -> VSMC-NS (DKD)
dEC -> EC-GC (Ref)
dEC -> EC-GC (DKD)
dEC -> prEC (Ref)
dEC -> prEC (DKD)
dEC -> dEC (Ref)
dEC -> dEC (DKD)
dEC -> EC-NS (Ref)
dEC -> EC-NS (DKD)
dEC -> MC (Ref)
dEC -> MC (DKD)
dEC -> VSMC-NS (Ref)
dEC -> VSMC-NS (DKD)
EC-NS -> EC-GC (Ref)
EC-NS -> EC-GC (DKD)
EC-NS -> prEC (Ref)
EC-NS -> prEC (DKD)
EC-NS -> dEC (Ref)
EC-NS -> dEC (DKD)
EC-NS -> EC-NS (Ref)
EC-NS -> EC-NS (DKD)
EC-NS -> MC (Ref)
EC-NS -> MC (DKD)
EC-NS -> VSMC-NS (Ref)
EC-NS -> VSMC-NS (DKD)
Commun. Prob.
max
min
p-value
p > 0.05
0.01 < p < 0.05
p < 0.01
B
Density
0.075
0.050
0.025
0.000
NPHS2
PECAM1
TAGLN
SEMA6A
PLXNA2
Density ratio
3
2
1
0
SEMA6A / PECAM1
Density ratio
0.3
0.2
0.1
0.0
PLXNA2 / (PECAM1 + TAGLN)
Condition
Ref
DKD
C
100 µm
100 µm
PECAM1
PLXNA2
SEMA6A
TAGLN
D
Reference
DKD
VEGFA
2
1
0
E
Target interactions
FN1 - SDC4
FN1 - CD44
FN1 - (ITGAV+ITGB8)
FN1 - (ITGAV+ITGB1)
FN1 - (ITGA8+ITGB1)
FN1 - (ITGA5+ITGB1)
FN1 - (ITGA4+ITGB1)
FN1 - (ITGA3+ITGB1)
WNT2B - (FZD6+LRP6)
WNT2B - (FZD4+LRP6)
WNT2B - (FZD4+LRP5)
prEC -> POD (Ref)
prEC -> POD (DKD)
prEC -> EC-GC (Ref)
prEC -> EC-GC (DKD)
prEC -> prEC (Ref)
prEC -> prEC (DKD)
prEC -> dEC (Ref)
prEC -> dEC (DKD)
prEC -> EC-NS (Ref)
prEC -> EC-NS (DKD)
prEC -> MC (Ref)
prEC -> MC (DKD)
prEC -> VSMC-NS (Ref)
prEC -> VSMC-NS (DKD)
prEC -> dVSMC (Ref)
prEC -> dVSMC (DKD)
F
Target interactions
JAG2 - NOTCH4
JAG2 - NOTCH3
JAG2 - NOTCH2
JAG2 - NOTCH1
JAG1 - NOTCH4
JAG1 - NOTCH3
JAG1 - NOTCH2
JAG1 - NOTCH1
DLL4 - NOTCH4
DLL4 - NOTCH3
DLL4 - NOTCH2
DLL4 - NOTCH1
prEC -> POD (Ref)
prEC -> POD (DKD)
prEC -> EC-GC (Ref)
prEC -> EC-GC (DKD)
prEC -> prEC (Ref)
prEC -> prEC (DKD)
prEC -> dEC (Ref)
prEC -> dEC (DKD)
prEC -> EC-NOS (Ref)
prEC -> EC-NOS (DKD)
prEC -> MC (Ref)
prEC -> MC (DKD)
prEC -> VSMC-NOS (Ref)
prEC -> VSMC-NOS (DKD)
prEC -> dVSMC (Ref)
prEC -> dVSMC (DKD)
Commun. Prob.
max
min
p-value
p > 0.05
p < 0.01

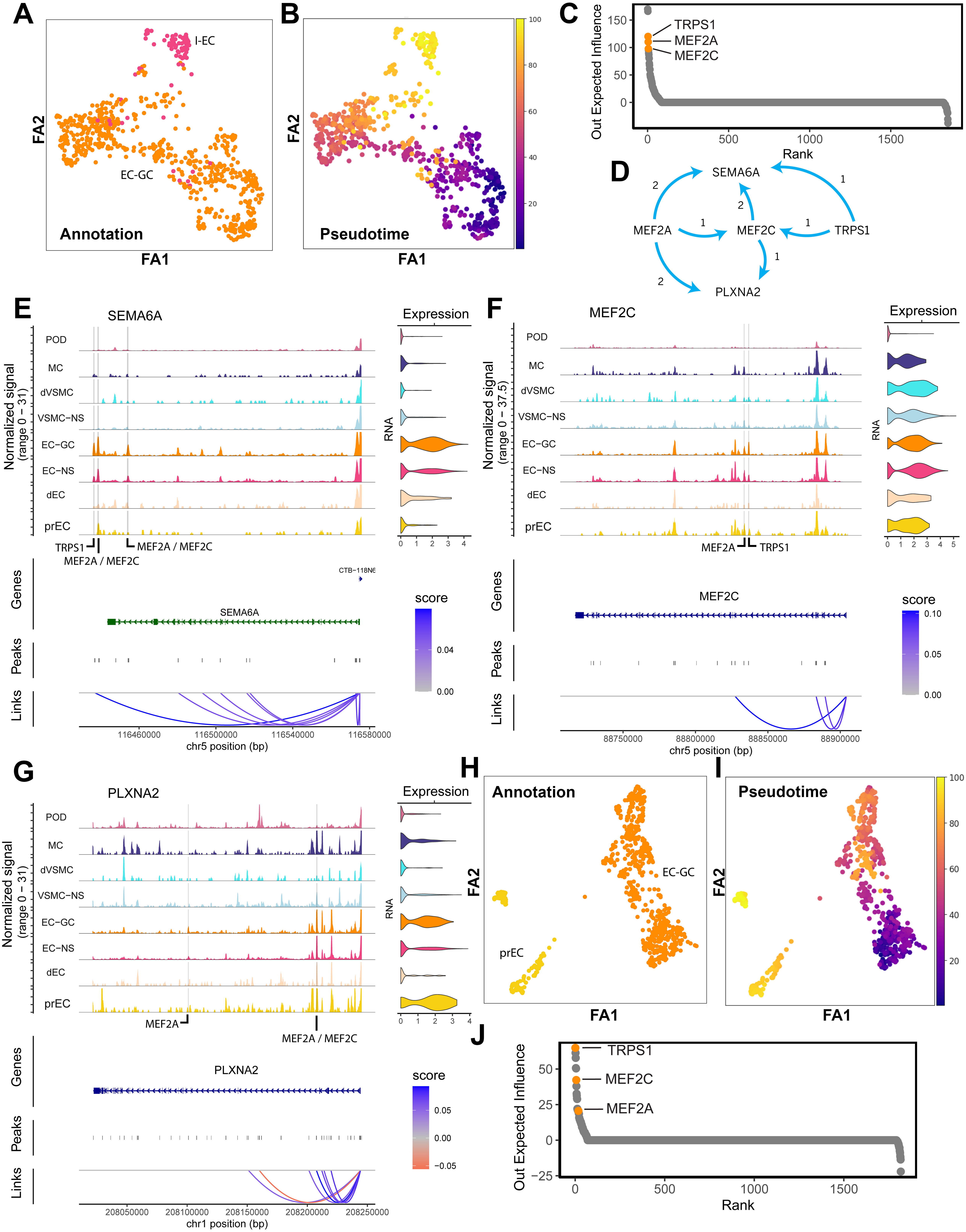
A
I-EC
EC-GC
Annotation
FA2
FA1
B
Pseudotime
FA2
FA1
100
80
60
40
20
C
Out Expected Influence
150
100
50
0
TRPS1
MEF2A
MEF2C
0
500
1000
1500
Rank
D
SEMA6A
MEF2A
MEF2C
TRPS1
PLXNA2
2
2
1
1
1
1
2
E
SEMA6A
Expression
Normalized signal
(range 0 – 31)
POD
MC
dVSMC
VSMC–NS
EC–GC
EC–NS
dEC
prEC
RNA
0
1
2
3
4
TRPS1
MEF2A / MEF2C
MEF2A / MEF2C
CTB-118N6
Genes
SEMA6A
Peaks
Links
score
0.04
0.00
116460000
116500000
116540000
116580000
chr5 position (bp)
F
MEF2C
Expression
Normalized signal
(range 0 – 37.5)
POD
MC
dVSMC
VSMC–NS
EC–GC
EC–NS
dEC
prEC
RNA
0
1
2
3
4
5
MEF2A
TRPS1
Genes
MEF2C
Peaks
Links
score
0.10
0.05
0.00
88750000
88800000
88850000
88900000
chr5 position (bp)
G
PLXNA2
Expression
Normalized signal
(range 0 – 31)
POD
MC
dVSMC
VSMC–NS
EC–GC
EC–NS
dEC
prEC
RNA
0
1
2
3
4
MEF2A
MEF2A / MEF2C
Genes
PLXNA2
Peaks
Links
score
0.05
0.00
−0.05
208050000
208100000
208150000
208200000
208250000
chr1 position (bp)
H
Annotation
EC-GC
prEC
FA2
FA1
I
Pseudotime
FA2
FA1
100
80
60
40
20
J
Out Expected Influence
TRPS1
MEF2C
MEF2A
50
25
0
−25
0
500
1000
1500
Rank

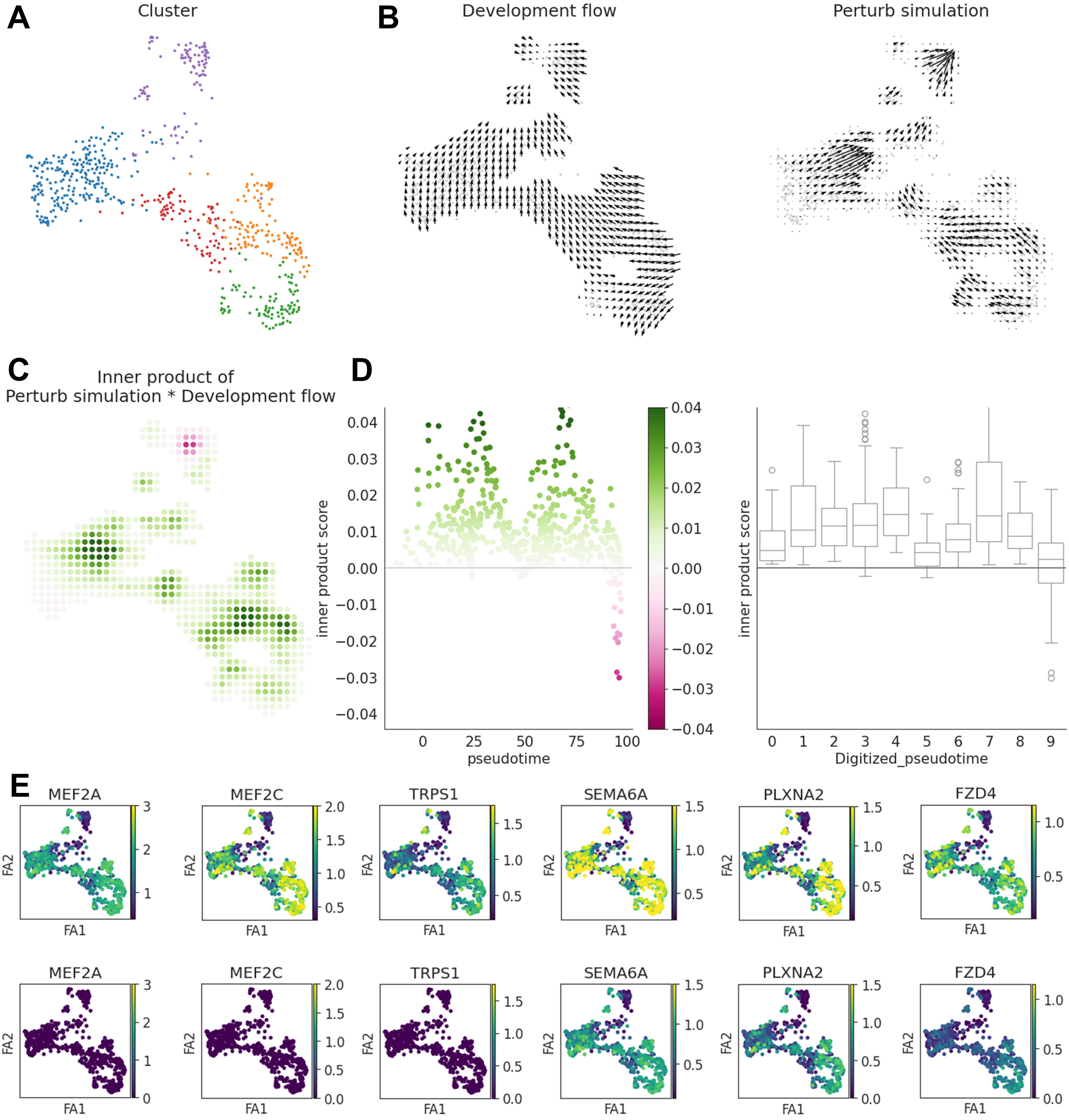
A
Cluster
B
Development flow
Perturb simulation
C
Inner product of
Perturb simulation * Development flow
D
inner product score
pseudotime
0.04
0.03
0.02
0.01
0.00
−0.01
−0.02
−0.03
−0.04
0
25
50
75
100
inner product score
Digitized_pseudotime
0
1
2
3
4
5
6
7
8
9
E
MEF2A
MEF2C
TRPS1
SEMA6A
PLXNA2
FZD4
FA1
FA2

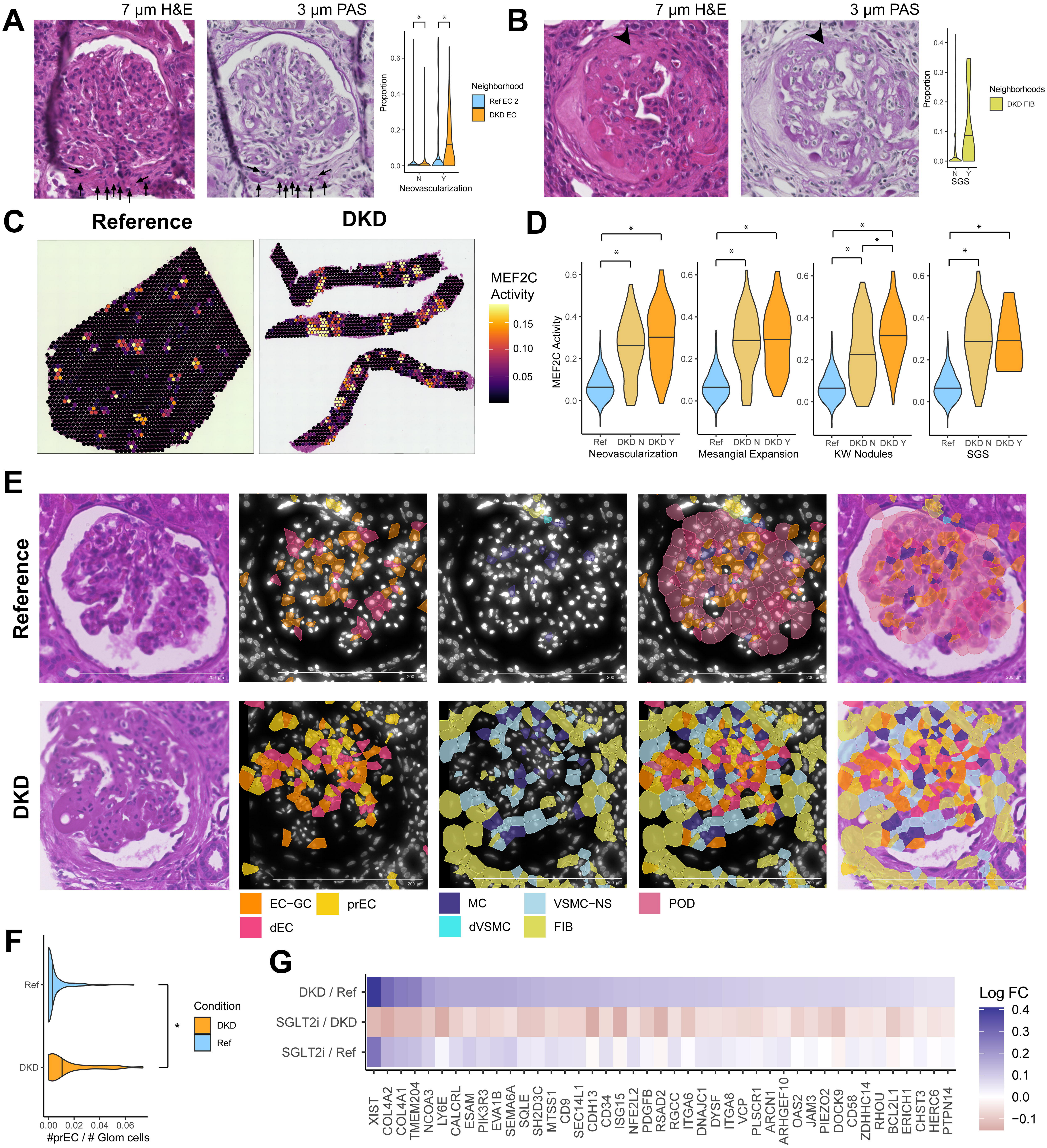
A
7 µm H&E
3 µm PAS
*
*
0.6
0.4
0.2
0.0
Proportion
N
Y
Neovascularization
Neighborhood
Ref EC 2
DKD EC
B
7 µm H&E
3 µm PAS
0.4
0.3
0.2
0.1
0.0
Proportion
N
Y
SGS
Neighborhoods
DKD FIB
C
Reference
DKD
MEF2C Activity
0.15
0.10
0.05
D
MEF2C Activity
0.6
0.4
0.2
0.0
*
Ref
DKD N
DKD Y
Neovascularization
Mesangial Expansion
KW Nodules
SGS
E
Reference
DKD
200 µm
EC−GC
prEC
dEC
MC
dVSMC
VSMC−NS
FIB
POD
F
Ref
DKD
*
Condition
DKD
Ref
0.00
0.02
0.04
0.06
#prEC / # Glom cells
G
DKD / Ref
SGLT2i / DKD
SGLT2i / Ref
Log FC
0.4
0.3
0.2
0.1
0.0
−0.1
XIST
COL4A2
COL4A1
TMEM204
NCOA3
LY6E
CALCRL
ESAM
PIK3R3
EVA1B
SEMA6A
SQLE
SH2D3C
MTSS1
CD9
SEC14L1
CDH13
CD34
ISG15
NFE2L2
PDGFB
RSAD2
RGCC
ITGA6
DNAJC1
DYSF
ITGA8
VCP
PLSCR1
ARCN1
ARHGEF10
OAS2
JAM3
PIEZO2
DOCK9
CD58
ZDHHC14
RHOU
BCL2L1
ERICH1
CHST3
HERC6
PTPN14

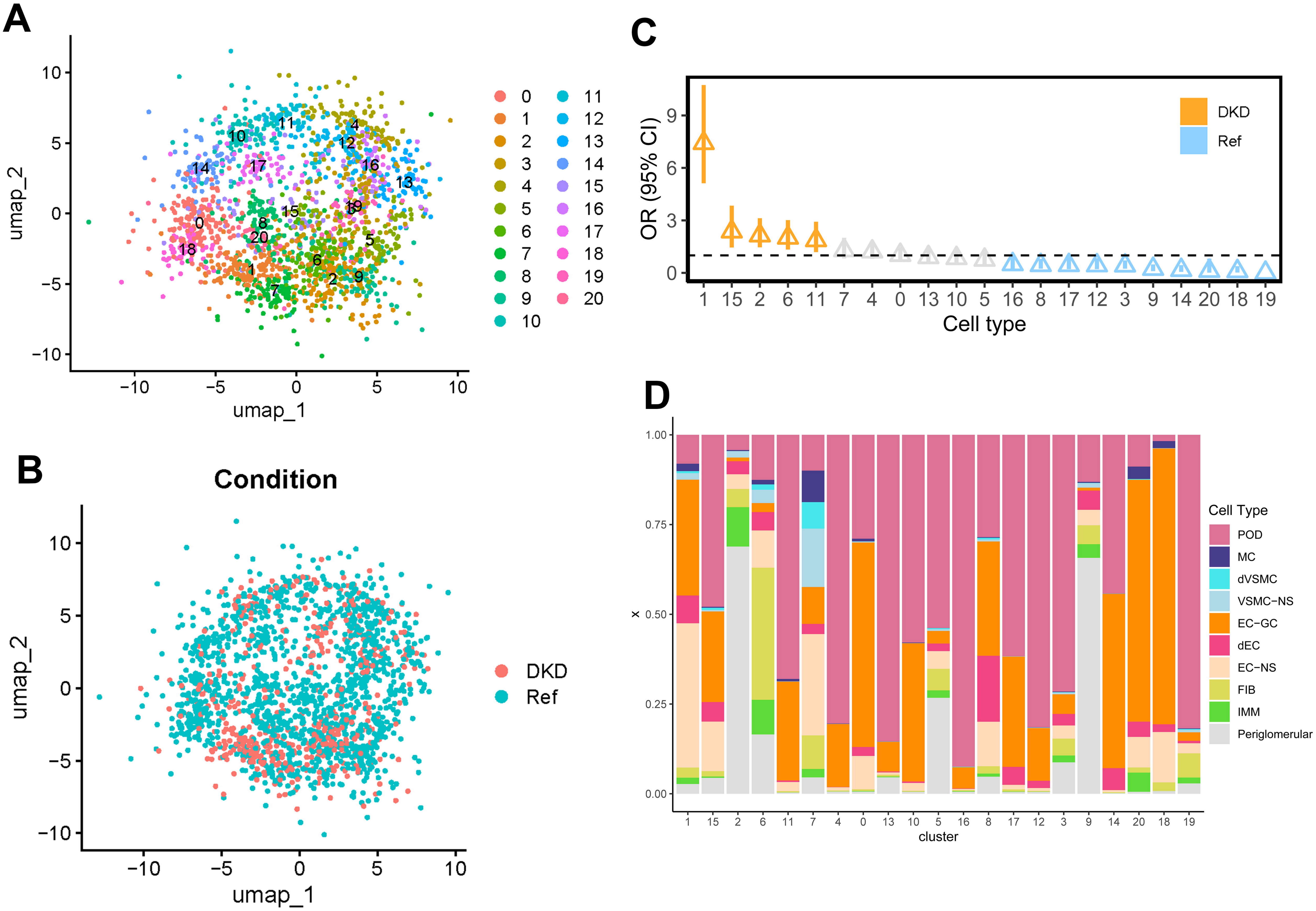
A
umap_2
umap_1
10
5
0
−5
−10
−10
−5
0
5
10
0
1
2
3
4
5
6
7
8
9
10
11
12
13
14
15
16
17
18
19
20
B
Condition
umap_2
umap_1
DKD
Ref
C
OR (95% CI)
9
6
3
0
DKD
Ref
1
15
2
6
11
7
4
0
13
10
5
16
8
17
12
3
9
14
20
18
19
Cell type
D
x
1.00
0.75
0.50
0.25
0.00
1
15
2
6
11
7
4
0
13
10
5
16
8
17
12
3
9
14
20
18
19
cluster
Cell Type
POD
MC
dVSMC
VSMC−NS
EC−GC
dEC
EC−NS
FIB
IMM
Periglomerular

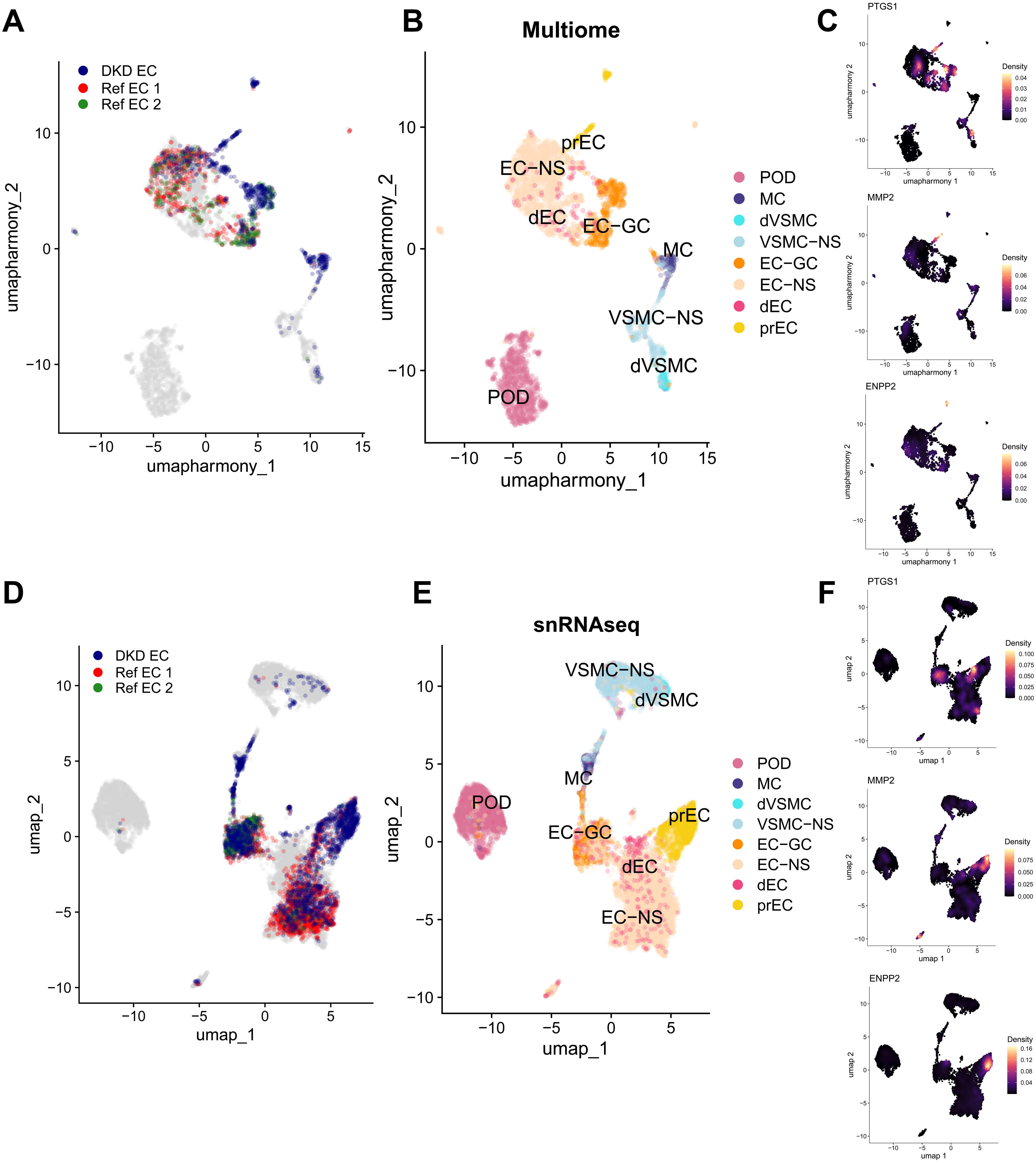
A
DKD EC
Ref EC 1
Ref EC 2
umapharmony_2
umapharmony_1
B
Multiome
prEC
EC−NS
dEC
EC−GC
MC
VSMC−NS
dVSMC
POD
umapharmony_2
umapharmony_1
POD
MC
dVSMC
VSMC−NS
EC−GC
EC−NS
dEC
prEC
C
PTGS1
MMP2
ENPP2
Density
umapharmony 2
umapharmony 1
D
DKD EC
Ref EC 1
Ref EC 2
umap_2
umap_1
E
snRNAseq
VSMC−NS
dVSMC
MC
POD
EC−GC
prEC
dEC
EC−NS
umap_2
umap_1
POD
MC
dVSMC
VSMC−NS
EC−GC
EC−NS
dEC
prEC
F
PTGS1
MMP2
ENPP2
Density
umap 2
umap 1

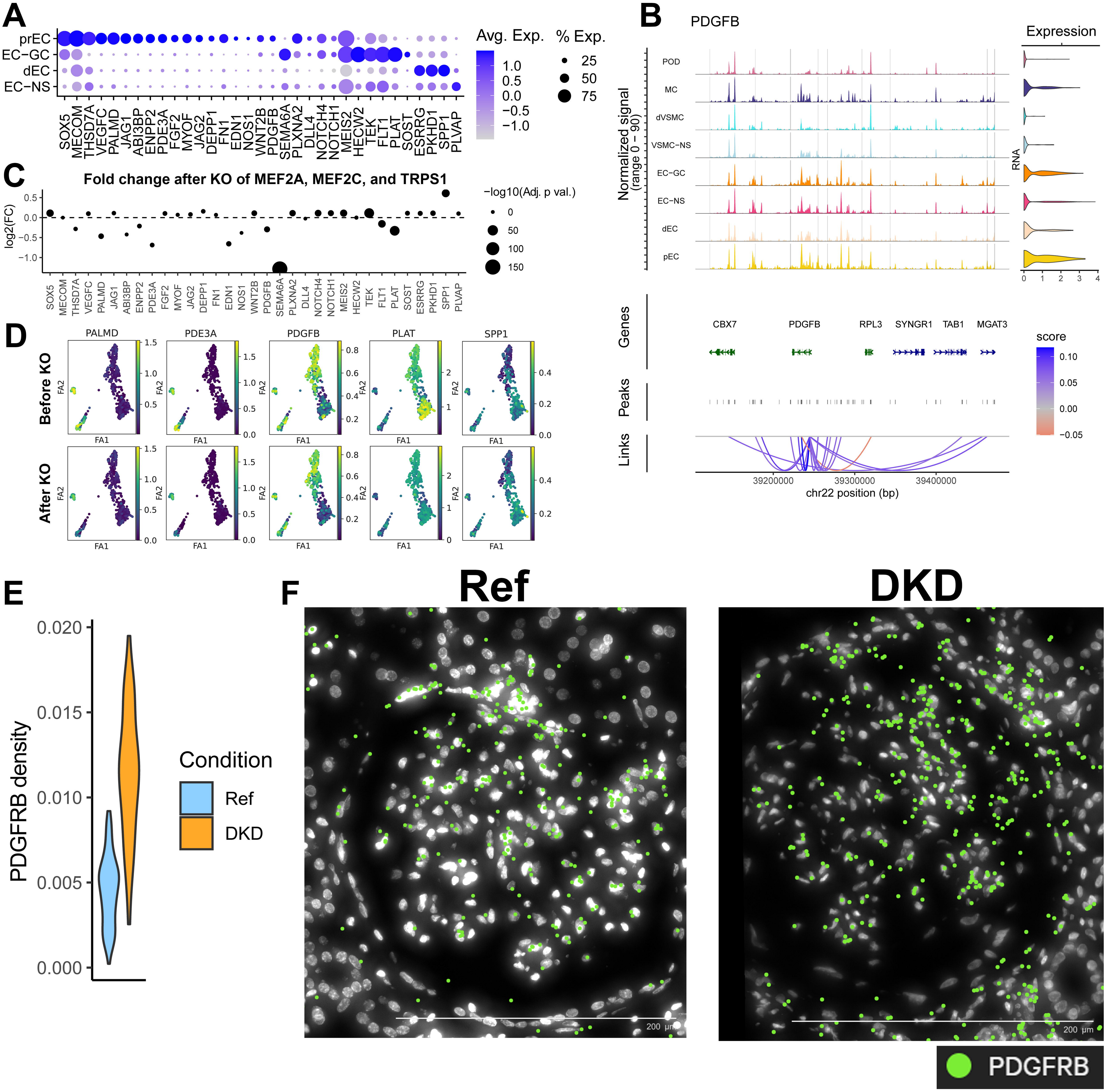
A
prEC
EC−GC
dEC
EC−NS
SOX5
MECOM
THSD7A
VEGFC
PALMD
JAG1
ABI3BP
ENPP2
PDE3A
FGF2
MYOF
JAG2
DEPP1
FN1
EDN1
NOS1
WNT2B
PDGFB
SEMA6A
PLXNA2
DLL4
NOTCH4
NOTCH1
MEIS2
HECW2
TEK
FLT1
PLAT
SOST
ESRRG
PKHD1
SPP1
PLVAP
Avg. Exp.
1.0
0.5
0.0
−0.5
−1.0
% Exp.
25
50
75
B
PDGFB
Normalized signal
(range 0 - 90)
POD
MC
dVSMC
VSMC-NS
EC-GC
EC-NS
dEC
pEC
Expression
RNA
0
1
2
3
4
Genes
CBX7
PDGFB
RPL3
SYNGR1
TAB1
MGAT3
Peaks
Links
score
0.10
0.05
0.00
−0.05
39200000
39300000
39400000
chr22 position (bp)
C
Fold change after KO of MEF2A, MEF2C, and TRPS1
log2(FC)
0.5
0.0
−0.5
−1.0
−log10(Adj. p val.)
0
50
100
150
SOX5
MECOM
THSD7A
VEGFC
PALMD
JAG1
ABI3BP
ENPP2
PDE3A
FGF2
MYOF
JAG2
DEPP1
FN1
EDN1
NOS1
WNT2B
PDGFB
SEMA6A
PLXNA2
DLL4
NOTCH4
NOTCH1
MEIS2
HECW2
TEK
FLT1
PLAT
SOST
ESRRG
PKHD1
SPP1
PLVAP
D
PALMD
PDE3A
PDGFB
PLAT
SPP1
Before KO
After KO
FA1
FA2
1.5
1.0
0.5
0.0
0.8
0.6
0.4
0.2
2
1
0
0.4
0.2
0.0
E
PDGFRB density
0.020
0.015
0.010
0.005
0.000
Condition
Ref
DKD
F
Ref
DKD
200 µm
200 µm
PDGFRB

A
MEF2A Knock out
Development flow
Perturb simulation
B
MEF2C Knock out
Development flow
Perturb simulation
C
TRPS1 Knock out
Development flow
Perturb simulation

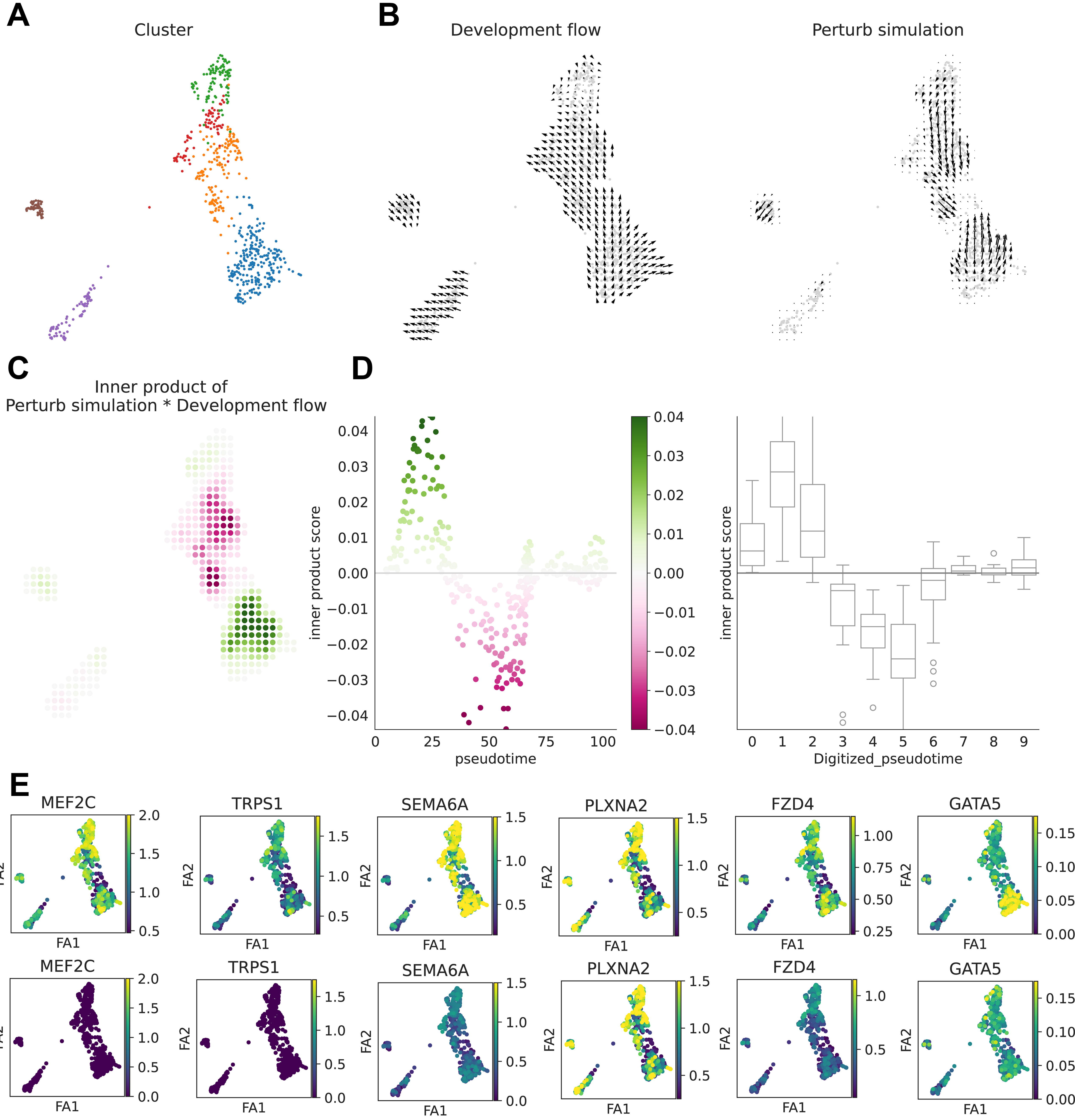
A
Cluster
B
Development flow
Perturb simulation
C
Inner product of
Perturb simulation * Development flow
D
inner product score
0.04
0.03
0.02
0.01
0.00
−0.01
−0.02
−0.03
−0.04
0
25
50
75
100
pseudotime
inner product score
0
1
2
3
4
5
6
7
8
9
Digitized_pseudotime
E
MEF2C
TRPS1
SEMA6A
PLXNA2
FZD4
GATA5
FA1
FA2
2.0
1.5
1.0
0.5
0.0
1.00
0.75
0.50
0.25
0.15
0.10
0.05
0.00

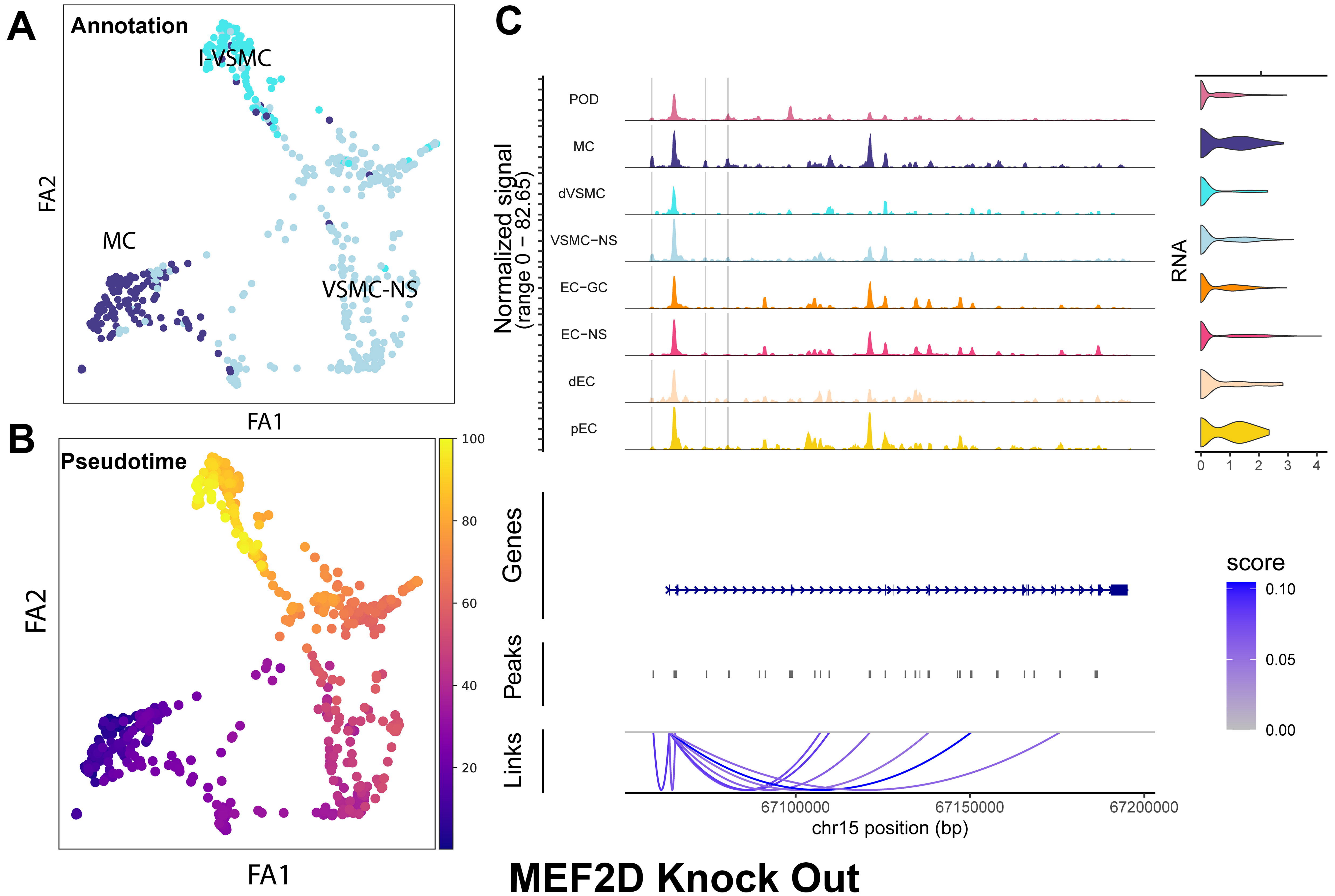

MEF2D Knock Out

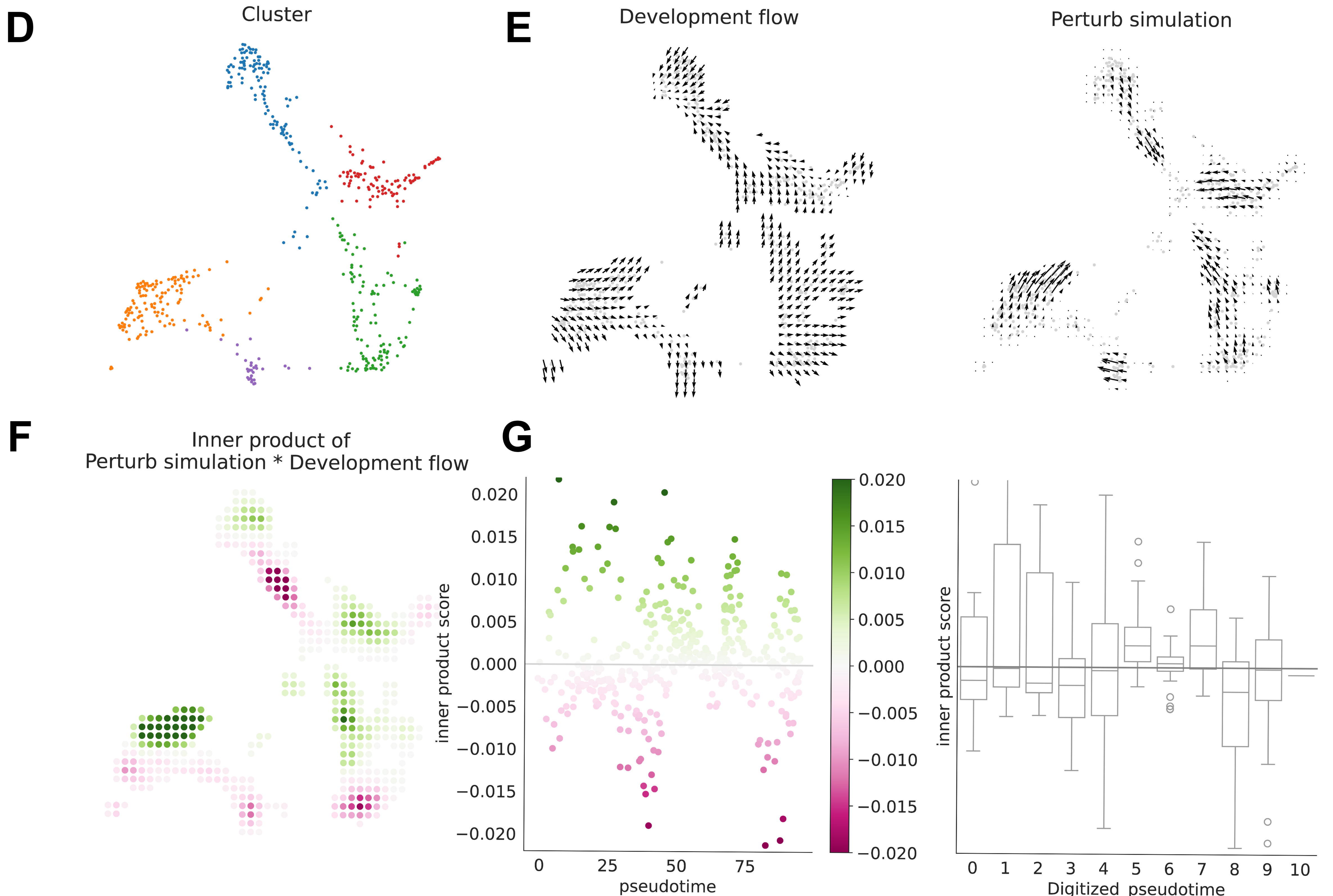

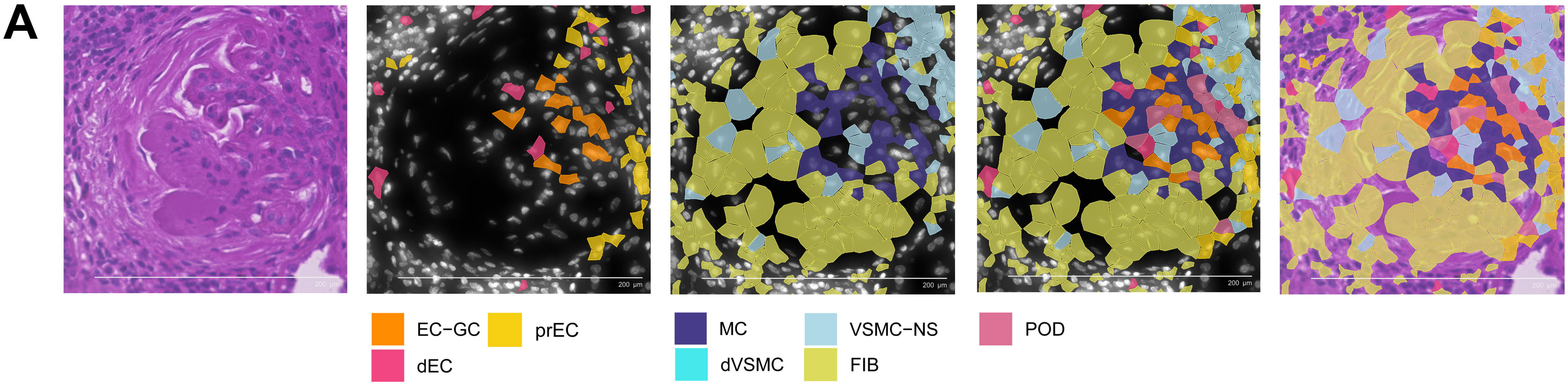
A
200 µm
200 µm
200 µm
200 µm
200 µm
EC−GC
prEC
dEC
MC
VSMC−NS
dVSMC
FIB
POD